International Journal of Solids and Structures 212 (2021) 152–168

Contents lists available at ScienceDirect

International Journal of Solids and Structures

journal homepage: www.elsevier.com/locate/ijsolstr

A variationally consistent formulation of the thermo-mechanically coupled problem with non-associative viscoplasticity for glassy amorphous polymers

Seishiro Matsubara [a,*], Kenjiro Terada [b]

[a] Department of Mechanical Systems Engineering, Nagoya University, Furo-cho, Chikusa-ku, Nagoya 464-8603, Japan
[b] International Research Institute of Disaster Science, Tohoku University, Aza-Aoba 468-1, Aramaki, Aoba-ku, Sendai 980-8572, Japan

ARTICLE INFO

Article history:
Received 28 July 2020
Received in revised form 29 October 2020
Accepted 5 December 2020
Available online 16 December 2020

Keywords:
Thermo-mechanics
Incremental variational formulation
Non-associative viscoplasticity
Glassy amorphous polymers

ABSTRACT

This study presents a variationally consistent formulation of the thermo-mechanically coupled problem with non-associative viscoplasticity for glassy amorphous polymers. First, the decomposition of the equivalent plastic strain is carried out to derive the variational consistent evolution law of the shear yield strength with reference to the analogous approach taken for formulating the Armstrong-Frederick model. Second, an alternative form of the dual viscoplastic dissipation potential is proposed to recast the principle of maximum plastic dissipation for viscoplasticity to be of the same form of rate-independent plasticity with the introduction of the extended yield function. Third, we address the optimization problem relevant to the thermo-mechanically coupled behavior of glassy amorphous polymers within the incremental variational framework with the help of the parameterization of flow rules. Thanks to the achieved variational consistency, the mathematical model derived by the proposed formulation can enjoy several benefits for ensuring the stability of the strongly coupled discretized equations in the monolithic method under the condition that the material behavior is stable. In addition, since the present formulation does not require the time derivative of the shear yield strength, the resulting evolution equation accommodates the time variations of temperature in terms of its material properties, implying that it is amenable to various thermal processes other than isothermal ones. Numerical examples are presented to demonstrate the capability of the proposed formulation in simulating actual compression tests conducted on a PMMA specimen that exhibits complex thermo-mechanically coupled phenomena.

1. Introduction

Inspired by Haward and Thackray (1968), a great deal of phenomenological constitutive models for glassy amorphous polymers have been proposed for about five decades. The fundamental feature on their compositions is that the physical bases are classified into intermolecular and entropic resistances. The former is commonly represented by evolution laws of the viscoplastic strain and the shear yield strength, and the latter has an affinity for hyperelasticity or kinematic hardening. For modeling the intermolecular resistance, two major approaches have been taken (Ward and Sweeney, 2013). One takes the line of classical crystal plasticity, and the constitutive models proposed by Argon (1973), Boyce et al. (1988a) and Anand and Gurtin (2003) are of this type. The other is based on the Eyring equation, which describes a thermally activated rate process of polymers; see, for example, Fotheringham and Cherry (1978) and Richeton et al. (2005, 2006, 2007) for relevant models. On the other hand, the entropic resistance is often represented by the so-called non-Gaussian network models with an eye on the analogy to rubber elasticity (Arruda and Boyce, 1993a).

Most of the more recently proposed constitutive models have been developed with a view to an application to thermo-mechanically coupled analysis; see, e.g., Arruda et al. (1995), Anand et al. (2009), Ames et al. (2009), Srivastava et al. (2010), Bouvard et al. (2013). Quite naturally, the 2nd law of thermodynamics is satisfied by way of the standard thermodynamics-based formulation (Coleman and Noll, 1963; Coleman and Gurtin, 1967). However, most of them are irrelevant to the theory associated with the potential structure in inelasticity such as the principle of maximum plastic dissipation and as a result "variationally inconsistent" in the formulation of thermo-mechanically coupled problems. Such an inconsistency conduces asymmetry of the con-

* Corresponding author.
E-mail address: seishiro.matsubara@mae.nagoya-u.ac.jp (S. Matsubara).

https://doi.org/10.1016/j.ijsolstr.2020.12.004
0020-7683/

sistent tangent modulus and makes the controversy about the existence of optimized solutions wracked. For this reason, no studies have ever tried to conduct a strongly coupled thermo-mechanical analysis with the fully coupled thermo-mechanical material model for glassy amorphous polymers by using a monolithic scheme without any simplification. In addition, to our best knowledge, little attention has been given to how the entropy influences the thermo-mechanically coupled behavior.

To conduct variationally consistent formulation for the constitutive model of glassy amorphous polymers, we take notice of the incremental variational framework; see, for example, Carstensen et al. (2002), Comi et al. (1991), Comi and Perego (1995), Ortiz and Stainier (1999) for early developments. In this framework, instantaneous local equilibrium states in the vicinity of a material point in an inelastic continuum body are given as solutions of the optimization problem of the local energy rate with respect to the internal state variables. The framework has already been extended to viscoelastic problem (Fancello et al., 2006, 2008), multiscale problems (Balzani and Ortiz, 2012; Bleier and Mosler, 2013), a novel numerical algorithm with hyper dual numbers (Tanaka et al., 2016), and thermo-mechanically coupled problems (Yang et al., 2005; Stainier and Ortiz, 2010). Notably, Mosler and Bruhns (2010) made a correlation between the flow vectors and yield function to establish the variationally consistent rate-independent plasticity model by parameterizing the direction of plastic flow with the introduction of 'pseudo' stress. Thanks to this "parameterization" strategy for flow rules, non-associative rate-independent plasticity models can also be made variationally consistent; see, for example, Mosler and Bruhns (2008) for the Drucker-Prager model, Mosler (2010) for the nonlinear kinematic hardening model and Canadija and Mosler (2011, 2016) for the thermo-mechanically coupled problems.

However, the variationally consistent formulation for glassy amorphous polymers requires some creative thinking. The major issue is that the derivation of the evolution law of the shear yield strength has hitherto been ignored within thermodynamics framework since it was originally proposed by Boyce et al. (1988a). It is, nevertheless, realized that it can be derived with reference to the mathematical structure of the Armstrong-Frederick model (Vladimirov et al., 2007; Henann and Anand, 2008; Vladimirov et al., 2010). In this context, its formulation is roughly classified into Chaboche's type (Chaboche, 1986, 1989) and Lion's type (Lion, 1999), which employs the plastic potential and the decomposition of plastic deformation, respectively; see Dettmer and Reese (2003) for a comparative study. But, for either of these types, another issue arises in deriving the variational consistent evolution law. That is, the resulting plasticity models are, unfortunately, "*non-associative*" and thus not aligned with the principle of maximum plastic dissipation. Hence, unless the incremental variational formulation for the non-associative viscoplasticity is developed, the analogous format to the Armstrong-Frederick model cannot be utilized to establish the variationally consistent formulation for glassy amorphous polymers.

With the aforementioned issues in mind, this study presents a variationally consistent formulation of the thermo-mechanically coupled problem with non-associative viscoplasticity for glassy amorphous polymers within the incremental variational framework. The main contribution of this study is not to pursue sophisticated material models for glassy amorphous polymers but to develop the new variationally consistent formulation for the thermo-mechanical coupled problem accommodating an arbitrary non-associative viscoplastic model based on the Perzyna type viscoplastic theory. To derive the variationally consistent evolution law of the shear yield strength, we begin with decomposing the equivalent plastic strain after the fashion of Lion (1999). We also propose an alternative form of the dual dissipation potential to recast the principle of maximum plastic dissipation for viscoplasticity, by which the variational consistency for non-associative viscoplasticity can be achieved with the help of the parameterization of the flow rule. Then, we establish the optimization problem relevant to the thermo-mechanically coupled behavior of glassy amorphous polymers within the incremental variational framework. Thanks to having the variational structure, the mathematical model derived by the proposed formulation can enjoy benefits for ensuring the stability of the strongly coupled discretized equations in the monolithic method under the condition that the material behavior is stable. Also, the present formulation does not require the time derivative of the shear yield strength, so that the target material behavior is not limited to isothermal cases; that is, applicable to the temperature change in time. A numerical simulation of the compression tests for Polymethyl-methacrylate (PMMA) reported in Arruda et al. (1995) is carried out to demonstrate the capability of the proposed formulation in simulating its complex thermo-mechanical behavior in an efficient way.

The outline of this paper is as follows. In Section 2, after defining the thermodynamical strain-like variables, we make a thermodynamically consistent formulation in relation to the energy storage parts of the present constitutive model. In Section 3, to recast the principle of maximum plastic dissipation in the form of Legendre-Fenchel transformation, we propose an alternative form of dual viscoplastic dissipation potential with a view to application of the parameterization of flow rule. It is then revealed that the present formulation reproduces the evolution law of the shear yield strength proposed by Boyce et al. (1988a) when limited to the isothermal process. In Section 4, after outlining the general format of the incremental variational principle for thermo-mechanically coupled problems, we incorporate the present constitutive equations along with the parameterized flow rules into the established optimization problem. Finally, in Section 5, a numerical example is presented to simulate the characteristic thermo-mechanical behavior of a PMMA specimen subjected to compressive loading.

2. Constitutive modeling for energy storage components

2.1. Fundamentals

2.1.1. Internal state variables

Let $B_0 \subset \mathbb{R}^3$ be the reference configuration of a continuum body with smooth boundary ∂B_0 and $\boldsymbol{X} \in B_0$ be the material point at time $t_0 \geq 0$. Also, let $B_t \subset \mathbb{R}^3$ be the current configuration at time $t \geqslant t_0$, which is identified by the smooth motion $\boldsymbol{x} = \boldsymbol{\varphi}(\boldsymbol{X}, t) : B_0 \times [t_0, t] \to B_t$. Then, the deformation gradient is defined as

$$\boldsymbol{F} = \nabla_{\boldsymbol{X}} \boldsymbol{\varphi}(\boldsymbol{X}, t), \tag{1}$$

along with non-singular condition: $J = \det(\boldsymbol{F}) > 0$. In addition, its isochoric component $\bar{\boldsymbol{F}}$ is given by the Flory decomposition (Flory, 1961) as follows:

$$\bar{\boldsymbol{F}} = J^{-\frac{1}{3}} \boldsymbol{F}. \tag{2}$$

To define internal state variables, we introduce the Kröner-Lee decomposition (Kröner, 1960; Lee, 1969) as

$$\boldsymbol{F} = \boldsymbol{F}^{\mathrm{e}} \boldsymbol{F}^{\mathrm{vp}}, \tag{3}$$

where $\boldsymbol{F}^{\mathrm{e}}$ and $\boldsymbol{F}^{\mathrm{vp}}$ are the elastic and viscoplastic components of $\boldsymbol{F}$, respectively. On the assumption of viscoplastic incompressibility, $\det(\boldsymbol{F}^{\mathrm{vp}}) = 1$, the determinant of $\boldsymbol{F}^{\mathrm{e}}$ is identical to J. Here, we define the intermediate configuration $B^{\mathrm{vp}} \subset \mathbb{R}^3$ as a *mathematical* vicinity measured by $d\boldsymbol{X}^{\mathrm{vp}} = \boldsymbol{F}^{\mathrm{vp}} d\boldsymbol{X}$.

Meanwhile, to formulate the Armstrong-Frederick type evolution law for the back stress, Lion (1999) introduces the decomposi-

tion of the plastic deformation gradient into energy storage and dissipative components, by which the frame-indifference is automatically satisfied. In analogy with this, the equivalent plastic strain $\bar{\varepsilon}^{\mathrm{vp}}$ is decomposed to formulate the evolution law of the isotropic hardening, Specifically, we postulate the following additive decomposition:

$$\bar{\varepsilon}^{\mathrm{vp}} = \bar{\varepsilon}^{\mathrm{vp}}_{\mathrm{e}} + \bar{\varepsilon}^{\mathrm{vp}}_{\mathrm{p}}, \tag{4}$$

where $\bar{\varepsilon}^{\mathrm{vp}}$ is the internal state variable analogous to an accumulated plastic stain calculated from the plastic rate of deformation tensor as usual. Also, $\bar{\varepsilon}^{\mathrm{vp}}_{\mathrm{e}}$ and $\bar{\varepsilon}^{\mathrm{vp}}_{\mathrm{p}}$ are the storage and dissipative parts of $\bar{\varepsilon}^{\mathrm{vp}}$, respectively. Thus, the set of internal state variables $\boldsymbol{Z}$ is defined as

$$\boldsymbol{Z} = \left\{ \boldsymbol{F}^{\mathrm{vp}}, \bar{\varepsilon}^{\mathrm{vp}}, \bar{\varepsilon}^{\mathrm{vp}}_{\mathrm{p}} \right\}. \tag{5}$$

Here, $\boldsymbol{F}^{\mathrm{vp}}$ represents the viscoplastic deformation of glassy amorphous polymers and has the same definition as in the standard finite plasticity theory. Also, $\bar{\varepsilon}^{\mathrm{vp}}_{\mathrm{e}} = \bar{\varepsilon}^{\mathrm{vp}} - \bar{\varepsilon}^{\mathrm{vp}}_{\mathrm{p}}$ contributes to the increase of intermolecular resistance, whereas $\bar{\varepsilon}^{\mathrm{vp}}_{\mathrm{p}}$ suppresses the intermolecular resistance and induces the saturation of the shear yield strength.

Remark 1. The multiplicative decomposition of $\boldsymbol{F}^{\mathrm{vp}}$ leads to the Armstrong-Frederick type evolution law to represent the kinematic hardening, while our approach is solely for deriving the flow stress in isotropic hardening, which is equivalent to that of the shear yield strength of glassy amorphous polymers presented in the literature; see, e.g., Boyce et al. (1988a), Anand and Gurtin (2003) and Bouvard et al. (2013). As will be demonstrated below, the decomposition of the equivalent plastic strain is a key to realize the variationally consistent formulation.

2.1.2. Thermodynamics

With the above setting, we define the total free energy density:

$$\begin{aligned}\psi(\boldsymbol{F},\boldsymbol{Z},T) &= \inf_{\eta}\left\{e(\boldsymbol{F},\boldsymbol{Z},\eta) - T\eta\right\} \\ &= \psi^{\mathrm{e}}(\boldsymbol{F}^{\mathrm{e}},T) + \psi^{\mathrm{vp}}\left(\boldsymbol{F}^{\mathrm{vp}},\bar{\varepsilon}^{\mathrm{vp}}_{\mathrm{e}},T\right) + \psi^{\mathrm{h}}(T),\end{aligned} \tag{6}$$

where e, η and $T \in \mathbb{R}_+ \equiv \{\xi | \forall \boldsymbol{X} \in B_0, \forall t \to \xi(\boldsymbol{X},t) > 0, \xi \in \mathbb{R}\}$ are the internal energy density, the entropy density and the absolute temperature, respectively. Also, ψ^{e}, ψ^{vp} and ψ^{h} are the elastic, viscoplastic and pure thermal components of the free energy density, respectively. Here, ψ^{vp} is the viscoplastic stored energy that generates the thermodynamic stresses associated with the viscoplastic hardening.

According to the conventional procedure (Coleman and Noll, 1963; Coleman and Gurtin, 1967), the total energy dissipation in B_0 is given as

$$D = \boldsymbol{P} : \dot{\boldsymbol{F}} - \rho_0\left(\dot{\psi} + \dot{T}\eta\right) + \boldsymbol{G}\cdot\boldsymbol{Q}, \tag{7}$$

where $\rho_0, \boldsymbol{P}, \boldsymbol{G} \equiv -(\nabla_{\boldsymbol{X}} T)/T$ and $\boldsymbol{Q}$ are the initial mass density, 1st Piola–Kirchhoff stress, normalized temperature gradient and the heat flux, respectively. In consideration of the hyperelastic constitutive law $\boldsymbol{P} = \partial_{\boldsymbol{F}}(\rho_0\psi)$ and the equation for entropy density $\eta = -\partial_T\psi$, the substitution of the material time derivative of (6) into (7) yields

$$D = \underbrace{\boldsymbol{M}^{\mathrm{eff}} : \boldsymbol{l}^{\mathrm{vp}} + q^{\mathrm{vp}}\dot{\bar{\varepsilon}}^{\mathrm{vp}} + q^{\mathrm{vp}}_{\mathrm{p}}\dot{\bar{\varepsilon}}^{\mathrm{vp}}_{\mathrm{p}}}_{=D^{\mathrm{vp}}} + \underbrace{\boldsymbol{G}\cdot\boldsymbol{Q}}_{=D^{\mathrm{h}}}, \tag{8}$$

where we have established the following definitions of the thermodynamic stresses energetically conjugate to $\boldsymbol{Z}$:

$$\boldsymbol{M}^{\mathrm{eff}} \equiv (\boldsymbol{F}^{\mathrm{e}})^{\mathrm{T}}\partial_{\boldsymbol{F}^{\mathrm{e}}}(\rho_0\psi^{\mathrm{e}}) - \partial_{\boldsymbol{F}^{\mathrm{vp}}}(\rho_0\psi^{\mathrm{vp}})(\boldsymbol{F}^{\mathrm{vp}})^{\mathrm{T}} = \boldsymbol{M} - \boldsymbol{M}^{\mathrm{back}}, \tag{9}$$

$$q^{\mathrm{vp}} \equiv -\partial_{\bar{\varepsilon}^{\mathrm{vp}}}(\rho_0\psi^{\mathrm{vp}}), \tag{10}$$

$$q^{\mathrm{vp}}_{\mathrm{p}} \equiv -\partial_{\bar{\varepsilon}^{\mathrm{vp}}_{\mathrm{p}}}(\rho_0\psi^{\mathrm{vp}}). \tag{11}$$

Here, $\boldsymbol{l}^{\mathrm{vp}} = \dot{\boldsymbol{F}}^{\mathrm{vp}}(\boldsymbol{F}^{\mathrm{vp}})^{-1}$, $\boldsymbol{M} \equiv (\boldsymbol{F}^{\mathrm{e}})^{\mathrm{T}}\partial_{\boldsymbol{F}^{\mathrm{e}}}(\rho_0\psi^{\mathrm{e}})$ and $\boldsymbol{M}^{\mathrm{back}} \equiv \partial_{\boldsymbol{F}^{\mathrm{vp}}}(\rho_0\psi^{\mathrm{vp}})(\boldsymbol{F}^{\mathrm{vp}})^{\mathrm{T}}$ are the viscoplastic velocity gradient, Mandel stress and back stress, respectively.

2.2. Specification of free energies

2.2.1. Elastic contribution

Assuming elastic isotropy, we decompose the elastic part of free energy as

$$\psi^{\mathrm{e}}(\boldsymbol{F}^{\mathrm{e}},T) = \psi^{\mathrm{e}}_{\mathrm{vol}}(\ln J,T) + \psi^{\mathrm{e}}_{\mathrm{dev}}\left(\bar{\boldsymbol{\varepsilon}}^{\mathrm{e}}_{\mathrm{H}},T\right), \tag{12}$$

where $\psi^{\mathrm{e}}_{\mathrm{vol}}$ and $\psi^{\mathrm{e}}_{\mathrm{dev}}$ are the volumetric and deviatoric components, respectively. Here, the isochoric part of elastic right Hencky strain defined as $\bar{\boldsymbol{\varepsilon}}^{\mathrm{e}}_{\mathrm{H}} = \frac{1}{2}\ln\left(\bar{\boldsymbol{C}}^{\mathrm{e}}\right)$ is used as an argument of $\psi^{\mathrm{e}}_{\mathrm{dev}}$ instead of the corresponding right Cauchy Green deformation tensor $\bar{\boldsymbol{C}}^{\mathrm{e}} = (\bar{\boldsymbol{F}}^{\mathrm{e}})^{\mathrm{T}}\bar{\boldsymbol{F}}^{\mathrm{e}}$; see Matsubara et al. (2020) for reference. Then, the hyperelastic constitutive equation is re-written as

$$\boldsymbol{P} = \partial_{\boldsymbol{F}}\left(\rho_0\psi^{\mathrm{e}}_{\mathrm{vol}}\right) + \partial_{\boldsymbol{F}}\left(\rho_0\psi^{\mathrm{e}}_{\mathrm{dev}}\right) = \tau^{\mathrm{vol}}\boldsymbol{F}^{-\mathrm{T}} + (\boldsymbol{F}^{\mathrm{e}})^{-\mathrm{T}}\boldsymbol{M}^{\mathrm{dev}}(\boldsymbol{F}^{\mathrm{vp}})^{-\mathrm{T}}, \tag{13}$$

with $\tau^{\mathrm{vol}} = \partial_{\ln J}\left(\rho_0\psi^{\mathrm{e}}_{\mathrm{vol}}\right)$ being the volumetric Kirchhoff stress. Also, since $\partial_{\bar{\boldsymbol{C}}^{\mathrm{e}}}\left(\rho_0\psi^{\mathrm{e}}_{\mathrm{dev}}\right)$ is co-axial to $\bar{\boldsymbol{C}}^{\mathrm{e}}$, $\boldsymbol{M}$ can be transformed as

$$\begin{aligned}\boldsymbol{M} &= (\boldsymbol{F}^{\mathrm{e}})^{\mathrm{T}}\partial_{\boldsymbol{F}^{\mathrm{e}}}\left(\rho_0\psi^{\mathrm{e}}_{\mathrm{dev}}\right) = \boldsymbol{M}^{\mathrm{dev}} = \boldsymbol{I}^{\mathrm{dev}} : \bar{\boldsymbol{C}}^{\mathrm{e}}\left\{2\partial_{\bar{\boldsymbol{C}}^{\mathrm{e}}}\left(\rho_0\psi^{\mathrm{e}}_{\mathrm{dev}}\right)\right\} \\ &= \boldsymbol{I}^{\mathrm{dev}} : \partial_{\bar{\boldsymbol{\varepsilon}}^{\mathrm{e}}_{\mathrm{H}}}\left(\rho_0\psi^{\mathrm{e}}_{\mathrm{dev}}\right),\end{aligned} \tag{14}$$

where $\boldsymbol{I}^{\mathrm{dev}} \equiv \boldsymbol{I} - \frac{1}{3}\boldsymbol{1}\otimes\boldsymbol{1}$ and $\boldsymbol{I}$ are the fourth order deviator and identity tensors, respectively.

To further formulate the constitutive model for glassy amorphous polymers, we explicitly define the above-introduced elastic components of free energy as

$$\begin{aligned}\rho_0\psi^{\mathrm{e}}_{\mathrm{vol}}(\ln J,T) &= \tfrac{1}{2}K(T)(\ln J)^2 - 3K(T)\alpha_{\mathrm{th}}(T)\ln J, \\ \rho_0\psi^{\mathrm{e}}_{\mathrm{dev}}\left(\bar{\boldsymbol{\varepsilon}}^{\mathrm{e}}_{\mathrm{H}},T\right) &= G(T)\bar{\boldsymbol{\varepsilon}}^{\mathrm{e}}_{\mathrm{H}} : \bar{\boldsymbol{\varepsilon}}^{\mathrm{e}}_{\mathrm{H}},\end{aligned} \tag{15}$$

where $K(T)$ and $G(T)$ are the bulk and shear elastic moduli, respectively. Also, $\alpha_{\mathrm{th}}(T)$ is the coefficient of thermal expansion to characterize the thermal strain stemming from the increase in free volume. Thus, substituting Eq. (15) into $\tau^{\mathrm{vol}} = \partial_{\ln J}\left(\rho_0\psi^{\mathrm{e}}_{\mathrm{vol}}\right)$ and Eq. (14), we obtain the specific forms of the volumetric Kirchhoff stress and deviatoric part of Mandel stress as follows, respectively:

$$\tau^{\mathrm{vol}} = K(T)(\ln J - 3\alpha_{\mathrm{th}}(T)) \quad \text{and} \quad \boldsymbol{M}^{\mathrm{dev}} = 2G(T)\bar{\boldsymbol{\varepsilon}}^{\mathrm{e}}_{\mathrm{H}}, \tag{16}$$

the latter of which is symmetric thanks to the isotropy in elasticity.

2.2.2. Viscoplasticity

The viscoplastic parts of free energy density can also be decomposed as

$$\psi^{\mathrm{vp}}\left(\boldsymbol{F}^{\mathrm{vp}},\bar{\varepsilon}^{\mathrm{vp}}_{\mathrm{e}},T\right) = \psi^{\mathrm{vp}}_{\mathrm{iso}}\left(\bar{\varepsilon}^{\mathrm{vp}}_{\mathrm{e}},T\right) + \psi^{\mathrm{vp}}_{\mathrm{kin}}\left(\boldsymbol{F}^{\mathrm{vp}},T\right), \tag{17}$$

where $\psi^{\mathrm{vp}}_{\mathrm{iso}}$ and $\psi^{\mathrm{vp}}_{\mathrm{kin}}$ are the isotropic and kinematic hardening components of viscoplastic free energy density, respectively. In order to formulate the evolution law of the flow stress for isotropic hardening, which is equivalent to shear yield strength proposed by Boyce et al. (1988a) as mentioned in Remark 1, we define the following function form of the viscoplastic free energy:

$$\rho_0\psi^{\mathrm{vp}}_{\mathrm{iso}}\left(\bar{\varepsilon}^{\mathrm{vp}}_{\mathrm{e}},T\right) = \frac{h(T)}{2}\left(\bar{\varepsilon}^{\mathrm{vp}}_{\mathrm{e}}\right)^2 + s^0_{\mathrm{Y}}(T)\bar{\varepsilon}^{\mathrm{vp}}_{\mathrm{e}}, \tag{18}$$

where $h(T)$ and $s^0_{\rm Y}(T)$ are the hardening modulus and initial yield strength, respectively. Then, we substitute Eq. (18) into Eqs. (10) and (11) to have the following specific forms of scalar-valued thermodynamic stresses:

$$q^{\rm vp} = -h(T)\bar{\varepsilon}^{\rm vp}_{\rm e} - s^0_{\rm Y}(T) \quad \text{and} \quad q^{\rm vp}_{\rm p} = h(T)\bar{\varepsilon}^{\rm vp}_{\rm e} + s^0_{\rm Y}(T), \tag{19}$$

from which we come to see that $q^{\rm vp} = -q^{\rm vp}_{\rm p}$.

On the contrary, to define the orientation hardening rule, we employ the following free energy function proposed by Gent (1996):

$$\rho_0\psi^{\rm vp}_{\rm kin}(\boldsymbol{F}^{\rm vp}, T) = -\frac{\mu(T)}{2}J_{\rm m}(T)\ln\left(1 - \frac{\bar{I}^{\rm vp}_1 - 3}{J_{\rm m}(T)}\right) \quad \text{with} \quad \bar{I}^{\rm vp}_1 = \mathrm{tr}(\bar{\boldsymbol{b}}^{\rm vp}),\ \boldsymbol{b}^{\rm vp} = \boldsymbol{F}^{\rm vp}(\boldsymbol{F}^{\rm vp})^{\rm T}, \tag{20}$$

because it can generally be interpreted as the non-Gaussian type entropic elasticity in terms of the viscoplastic deformation (Boyce et al., 1988a). Such a modeling approach to the orientation hardening is common for the constitutive modelling of glassy amorphous polymers and indeed accepted in the literature (Boyce et al., 1988a; Anand and Gurtin, 2003). Here, $\mu(T)$ and $J_{\rm m}(T) > 3.0$ are the stiffness representing entropic resistance and the material parameter associated with the so-called limiting chain extensibility, respectively. It should be noted that, in order to ensure $\boldsymbol{M}^{\rm back}(\boldsymbol{F}^{\rm vp}, T)\big|_{\boldsymbol{F}^{\rm vp}=\boldsymbol{1}} = \boldsymbol{0}$, we have adopted the isochoric part of the viscoplastic left Cauchy-Green deformation tensor, $\bar{\boldsymbol{b}}^{\rm vp}$, as an independent variable of $\psi^{\rm vp}_{\rm kin}$, even though $\det(\boldsymbol{F}^{\rm vp}) = 1$ is assumed. Then, the back stress $\boldsymbol{M}^{\rm back}$ is given as follows:

$$\begin{aligned}\boldsymbol{M}^{\rm back} &= \partial_{\boldsymbol{F}^{\rm vp}}(\rho_0\psi^{\rm vp})(\boldsymbol{F}^{\rm vp})^{\rm T} = 2\partial_{\boldsymbol{b}^{\rm vp}}(\rho_0\psi^{\rm vp}_{\rm kin})\boldsymbol{b}^{\rm vp}\\ &= \mu(T)\left(1 - \frac{\bar{I}^{\rm vp}_1 - 3}{J_{\rm m}(T)}\right)^{-1}\boldsymbol{I}^{\rm dev} : \boldsymbol{b}^{\rm vp}.\end{aligned} \tag{21}$$

Obviously, $\boldsymbol{M}^{\rm back}$ exhibits symmetry and therefore the viscoplastic flow stress $\boldsymbol{M}^{\rm eff}$ is also symmetric by reference to Eq. (9).

2.2.3. Thermal effects

We define the function form of the thermal component of free energy as

$$\rho_0\psi^{\rm h}(T) = \rho_0 c\left\{T - T_0 - T\ln\left(\frac{T}{T_0}\right)\right\}, \tag{22}$$

where c and T_0 are the specific heat and ambient temperature, respectively. In view of Eq. (6), the entropy $\rho_0\eta$ can be expressed in the form of an additive decomposition as

$$\rho_0\eta = \rho_0\eta^{\rm e} + \rho_0\eta^{\rm vp} + \rho_0\eta^{\rm h}. \tag{23}$$

Here, $\rho_0\eta^{\rm e}, \rho_0\eta^{\rm vp}$ and $\rho_0\eta^{\rm h}$ are the entropies associated with elasticty, viscoplasticity and heat conduction, respectively, and obtained by using Eqns. (12), (15), (17), (18), (20) and (22) as

$$\begin{aligned}\rho_0\eta^{\rm e} &= -\partial_T K(T)\left(\tfrac{1}{2}\ln J - 3\alpha_{\rm th}(T)\right)\ln J + 3K(T)\partial_T\alpha_{\rm th}(T)\ln J\\ &\quad -\partial_T G(T)\bar{\boldsymbol{\varepsilon}}^{\rm e}_{\rm H} : \bar{\boldsymbol{\varepsilon}}^{\rm e}_{\rm H},\end{aligned} \tag{24}$$

$$\begin{aligned}\rho_0\eta^{\rm vp} &= -\tfrac{\partial_T h(T)}{2}\left(\bar{\varepsilon}^{\rm vp}_{\rm e}\right)^2 - \partial_T s^0_{\rm Y}(T)\bar{\varepsilon}^{\rm vp}_{\rm e}\\ &\quad + \tfrac{1}{2}\left(\partial_T\mu(T)J_{\rm m}(T) + \mu(T)\partial_T J_{\rm m}(T)\right)\ln\left(1 - \tfrac{\bar{I}^{\rm vp}_1 - 3}{J_{\rm m}(T)}\right)\\ &\quad + \tfrac{\mu(T)\partial_T J_{\rm m}(T)}{2J_{\rm m}(T)}\left(\bar{I}^{\rm vp}_1 - 3\right)\left(1 - \tfrac{\bar{I}^{\rm vp}_1 - 3}{J_{\rm m}(T)}\right)^{-1},\end{aligned} \tag{25}$$

$$\rho_0\eta^{\rm h} = \rho_0 c\ln\left(\tfrac{T}{T_0}\right). \tag{26}$$

Remark 2. If the non-Gaussian network models such as the Arruda-Boyce model (Arruda and Boyce, 1993a,b) is adopted instead of Eq. (20), unanticipated heat conduction occurs even under isothermal and no-load conditions. This is because, under these conditions, the corresponding entropy, $\eta_{\rm NG}(\boldsymbol{F}, T)\big|_{\boldsymbol{F}=\boldsymbol{1}, T=\text{const.}}$ has a non-zero value; i.e., the self-generated heat arises without any thermo-mechanical excitations. For this reason, we have employed the Gent model to represent the orientation hardening.

3. Variationally consistent flow rules for non-associative viscoplasticity

In this section, a dual dissipation potential for non-associative viscoplasticity is orignally formulated for glassy amorphous polymers by the introduction of the extended loading–unloading condition. By defining the plastic potential, we derive a specific function form of the dual dissipation potential and specifically define the flow rules for themodynamic strains associated with non-associative viscoplasticity in a variationally consistent manner. It is then demonstrated that the present flow rules naturally reproduce the evolution law of the shear yield strength that is proposed by Boyce et al. (1988a) when limited to the isothermal process.

3.1. Dual dissipation potential for non-associative viscoplasticity

Within the framework of the rate-independent plasticity theory for standard dissipative solids in the sense of Halphen and Nguyen (1975), the plastic dissipation potential $\hat{\varphi}^{\rm p}$ can be identified with the following indicator function with respect to the set of driving forces $\boldsymbol{Y}$, which is energetically conjugate to the set of extensive variables $\boldsymbol{Z}$ in plasticity:

$$\hat{\varphi}^{\rm p}(\boldsymbol{Y}) = \begin{cases} 0 & \text{if } \boldsymbol{Y} \in \Xi_\sigma \\ +\infty & \text{otherwise} \end{cases}. \tag{27}$$

Here, the admissible set of thermodynamic stresses $\Xi_\sigma = \{\boldsymbol{Y} | f(\boldsymbol{Y}) \leqslant 0\}$ defines the level set of the yield function f, which is supposed to be convex. Then, the Legendre-Fenchel transformation provides the corresponding support function $\varphi^{\rm p}$ as

$$\varphi^{\rm p}\left(\dot{\boldsymbol{Z}}\right) = \sup_{\forall \boldsymbol{Y}}\left[\boldsymbol{Y} * \dot{\boldsymbol{Z}} - \hat{\varphi}^{\rm p}(\boldsymbol{Y})\right], \tag{28}$$

which corresponds to the principle of maximum plastic dissipation, but is not subjected to the stress constraint thanks to the introduction of the indicator function (Simo and Hughes, 2006). In the light of the mathematical properties between the indicator and support functions, the plastic multiplier $\dot{\gamma}^{\rm p}$ is not related to the dissipation potential, but determined by the necessary condition for optimality such that $\dot{\gamma}^{\rm p} \geq 0, f(\boldsymbol{Y}) \leq 0$ and $\dot{\gamma}^{\rm p} f(\boldsymbol{Y}) = 0$, which is commonly referred to as the loading–unloading condition. In this case, the stationary condition, $\dot{\boldsymbol{Z}} = \dot{\gamma}^{\rm p}\partial_{\boldsymbol{Y}} f(\boldsymbol{Y})$, which is another necessary condition for optimality, is called "*associative*" flow rule.

On the other hand, in the associative rate-dependent or viscoplasticity theory, viscoplastic multiplier $\dot{\gamma}^{\rm vp}$ explicitly provided, because the viscoplastic dissipation potential $\hat{\varphi}^{\rm vp}$ is defined as a penalization function with the penalty parameter $\eta^{\rm vp}$ in the sense of Perzyna-type viscoplastic regularization; see, e.g., Simo and Hughes (2006). As a result, $f(\boldsymbol{Y}) > 0$ is acceptable, and $\dot{\gamma}^{\rm vp}$ is identified with

$$\dot{\gamma}^{\rm vp} = \partial_{f(\boldsymbol{Y})}\hat{\varphi}^{\rm vp} \geqslant 0, \tag{29}$$

which is derived as a stationary condition of Eq. (28), but is not accompanied by the aforementioned necessary condition postulat-

ing loading–unloading states. The specific expressions can be similar to those of the standard creep models; e.g., Norton's creep law.

Moreover, Eq. (29) can be rewritten as an extension of yield criteria of the following form:

$$\Pi(f(\boldsymbol{Y}),\Lambda(\dot{\gamma}^{\mathrm{vp}}))\equiv f(\boldsymbol{Y})-\Lambda(\dot{\gamma}^{\mathrm{vp}})=0, \tag{30}$$

where $\Lambda(\dot{\gamma}^{\mathrm{vp}})$ is often called the over stress. Then, it follows that

$$\text{If } f(\boldsymbol{Y})\leq 0 \text{ , then } \dot{\gamma}^{\mathrm{vp}}=0 \text{ and } \Lambda(\dot{\gamma}^{\mathrm{vp}})=0; \quad \Rightarrow \quad \Pi(f(\boldsymbol{Y}),\Lambda(\dot{\gamma}^{\mathrm{vp}}))\leqslant 0 \tag{31}$$

$$\text{If } f(\boldsymbol{Y})\geq 0, \text{ then } \dot{\gamma}^{\mathrm{vp}}\geqslant 0 \text{ and } \Lambda(\dot{\gamma}^{\mathrm{vp}})\geqslant 0; \quad \Rightarrow \quad \text{Eq. (30)} \tag{32}$$

and therefore the following condition holds:

$$\dot{\gamma}^{\mathrm{vp}}\geqslant 0,\Pi(f(\boldsymbol{Y}),\Lambda(\dot{\gamma}^{\mathrm{vp}}))\leqslant 0 \text{ and } \dot{\gamma}^{\mathrm{vp}}\Pi(f(\boldsymbol{Y}),\Lambda(\dot{\gamma}^{\mathrm{vp}}))=0. \tag{33}$$

which bears a close resemblance to the loading–unloading condition. In response to this fact, we define the 'pseudo' dual viscoplastic dissipation potential as

$$\tilde{\varphi}^{\mathrm{vp}}\left(\dot{\boldsymbol{Z}},\dot{\gamma}^{\mathrm{vp}}\right)=\sup_{\boldsymbol{Y}}\left[\boldsymbol{Y}*\dot{\boldsymbol{Z}}-\hat{\varphi}^{\mathrm{vp}}(\boldsymbol{Y},\dot{\gamma}^{\mathrm{vp}})\right] \tag{34}$$

in which the following 'pseudo' viscoplastic dissipation potential has been introduced:

$$\hat{\varphi}^{\mathrm{vp}}(\boldsymbol{Y},\dot{\gamma}^{\mathrm{vp}})=\begin{cases}0 & \text{if } \boldsymbol{Y}\in\tilde{\Xi}_{\sigma}\\ +\infty & \text{otherwise}\end{cases}, \tag{35}$$

Here, the admissible set of thermodynamic stresses, $\tilde{\Xi}_{\sigma}=\{\boldsymbol{Y}|\Pi(f(\boldsymbol{Y}),\Lambda(\dot{\gamma}^{\mathrm{vp}}))\leqslant 0\}$, defines the level set of convex functions Π. Thus, the principle of maximum dissipation for viscoplasticity has been expressed in accordance with the rate-independent plasticity theory. Also, the relevant stationary and loading–unloading conditions are given as, respectively,

$$\dot{\boldsymbol{Z}}=\dot{\lambda}^{\mathrm{vp}}\partial_{\boldsymbol{Y}}\Pi(f(\boldsymbol{Y}),\Lambda(\dot{\gamma}^{\mathrm{vp}}))=\dot{\lambda}^{\mathrm{vp}}\partial_{\boldsymbol{Y}}f(\boldsymbol{Y}), \tag{36}$$

$$\dot{\lambda}^{\mathrm{vp}}\geqslant 0,\ \Pi(f(\boldsymbol{Y}),\Lambda(\dot{\gamma}^{\mathrm{vp}}))\leqslant 0 \text{ and } \dot{\lambda}^{\mathrm{vp}}\Pi(f(\boldsymbol{Y}),\Lambda(\dot{\gamma}^{\mathrm{vp}}))=0, \tag{37}$$

where $\dot{\lambda}^{\mathrm{vp}}$ is an another viscoplastic multiplier. It follows that if the identify $\dot{\lambda}^{\mathrm{vp}}=\dot{\gamma}^{\mathrm{vp}}$ is imposed, the necessary conditions for optimality in the viscoplasticity theory are exactly reproduced. These redefinitions of the viscoplastic dissipation potentials make the viscoplastic multiplier $\dot{\gamma}^{\mathrm{vp}}$ irrelevant to the dissipation potential. In other words, $\dot{\gamma}^{\mathrm{vp}}$ is determined from Eq. (30) with Eq. (33) in place of Eq. (29). Hence, the 'pseudo' dual viscoplastic dissipation potential is expressed as

$$\tilde{\varphi}^{\mathrm{vp}}\left(\dot{\boldsymbol{Z}},\dot{\gamma}^{\mathrm{vp}}\right)=\boldsymbol{Y}*\dot{\boldsymbol{Z}} \tag{38}$$

regardless of $\hat{\varphi}^{\mathrm{vp}}$.

Within the framework of rate-independent plasticity with nonlinear kinematic hardening laws, a plastic potential $\Omega(\boldsymbol{Y})\geqslant 0$ is introduced separately from the yield function and is used to define the evolution equation of $\boldsymbol{Z}$ such that $\dot{\boldsymbol{Z}}=\dot{\gamma}^{\mathrm{p}}\partial_{\boldsymbol{Y}}\Omega(\boldsymbol{Y})$; see, e.g., Chaboche (1986), Chaboche (1989), Dettmer and Reese (2003), Vladimirov et al. (2007, 2010) and many others. As it is generally known, such a theory is called "*non-associative*" plasticity. On the other hand, for non-associative viscoplasticity, the stationary condition (Eq. (36)) in the redefined optimization problem is replaced with $\dot{\boldsymbol{Z}}=\dot{\lambda}^{\mathrm{vp}}\partial_{\boldsymbol{Y}}\Omega(\boldsymbol{Y})$, because viscoplastic dissipation potential $\hat{\varphi}^{\mathrm{vp}}$, which defines the loading–unloading condition (Eq. (37)), can not properly be defined. However, since the non-associative models do not satisfy the principle of maximum plastic dissipation, the 'pseudo' dual viscoplastic dissipation potential $\tilde{\varphi}^{\mathrm{vp}}$ cannot be defined. In this regard, Mosler and Bruhns (2008) and Mosler (2010) demonstrated that the optimization problem for non-associative models could be formulated by use of the plastic energy dissipation as the dual plastic dissipation potential if the homogeneous yield function is adopted for the rate-independent plasticity model. Based on this argument, the function form of $\tilde{\varphi}^{\mathrm{vp}}$ will be specified through the use of Eq. (38) in what follows.

We begin with differentiating both sides of Eq. (38) with respect to $\dot{\gamma}^{\mathrm{vp}}$ to obtain

$$\partial_{\dot{\gamma}^{\mathrm{vp}}}\tilde{\varphi}^{\mathrm{vp}}=\boldsymbol{Y}*\partial_{\dot{\gamma}^{\mathrm{vp}}}\dot{\boldsymbol{Z}}(\dot{\gamma}^{\mathrm{vp}}). \tag{39}$$

Then, assuming that $f(\boldsymbol{Y})$ is one-order homogeneous function with respect to $\boldsymbol{Y}$ that satisfies

$$f(\boldsymbol{Y})=\overline{Y}(\boldsymbol{Y})-\sigma_{\mathrm{Y}}^{0} \text{ with } \overline{Y}(\boldsymbol{Y})=\boldsymbol{Y}*\partial_{\boldsymbol{Y}}f, \tag{40}$$

we substitute Eq. (36) along with constraint $\dot{\lambda}^{\mathrm{vp}}=\dot{\gamma}^{\mathrm{vp}}$ into Eq. (39) to obtain

$$\partial_{\dot{\gamma}^{\mathrm{vp}}}\tilde{\varphi}^{\mathrm{vp}}=f(\boldsymbol{Y})+\sigma_{\mathrm{Y}}^{0}+\boldsymbol{Y}*\partial_{\boldsymbol{Y}}\Omega^{*}(\boldsymbol{Y}) \quad \text{with } \Omega^{*}(\boldsymbol{Y}) =\Omega(\boldsymbol{Y})-f(\boldsymbol{Y}). \tag{41}$$

Here, σ_{Y}^{0} is the initial yield stress. Replacing $f(\boldsymbol{Y})$ by $\Lambda(\dot{\gamma}^{\mathrm{vp}})$ with reference to Eq. (30) and integrating this expression with respect to $\dot{\gamma}^{\mathrm{vp}}$, the following 'pseudo' dual viscoplastic dissipation potential is provided:

$$\tilde{\varphi}^{\mathrm{vp}}(\dot{\gamma}^{\mathrm{vp}};\boldsymbol{Y})=\sigma_{\mathrm{Y}}^{0}\dot{\gamma}^{\mathrm{vp}}+\boldsymbol{Y}*\partial_{\boldsymbol{Y}}\Omega^{*}(\boldsymbol{Y})\dot{\gamma}^{\mathrm{vp}}+\int_{0}^{\dot{\gamma}^{\mathrm{vp}}}\Lambda\left(\hat{\dot{\gamma}}^{\mathrm{vp}}\right)d\hat{\dot{\gamma}}^{\mathrm{vp}}. \tag{42}$$

It will be demonstrated in the next section that the optimization problem for the continuum body is established by the application of the derived $\tilde{\varphi}^{\mathrm{vp}}$ to the incremental variational framework for non-associative plasticity (Mosler and Bruhns, 2008; Mosler, 2010).

3.2. Specification of viscoplastic flow evolutions

We specifically define the plastic potential as

$$\Omega\left(\boldsymbol{M}^{\mathrm{eff}},q^{\mathrm{vp}},q_{\mathrm{p}}^{\mathrm{vp}},T\right)=\Sigma_{\mathrm{dev}}^{\mathrm{eq}}\left(\boldsymbol{M}^{\mathrm{eff}}\right)+q^{\mathrm{vp}}+\frac{\left(q_{\mathrm{p}}^{\mathrm{vp}}\right)^{2}}{2s_{\mathrm{ss}}(T)} \quad \text{with} \quad \Sigma_{\mathrm{dev}}^{\mathrm{eq}}\left(\boldsymbol{M}^{\mathrm{eff}}\right)=\sqrt{\tfrac{1}{2}\boldsymbol{M}^{\mathrm{eff}}:\boldsymbol{M}^{\mathrm{eff}}}, \tag{43}$$

where $s_{\mathrm{ss}}(T)\leqslant s_{\mathrm{Y}}^{0}(T)$ is the peak yield strength at a zero pressure level (Boyce et al., 1988a). Here, recalling Eq. (8), the relevant flow rules are defined as $\boldsymbol{l}^{\mathrm{vp}}=\dot{\gamma}^{\mathrm{vp}}\partial_{\boldsymbol{M}^{\mathrm{eff}}}\Omega$, $\dot{\varepsilon}^{\mathrm{vp}}=\dot{\gamma}^{\mathrm{vp}}\partial_{q^{\mathrm{vp}}}\Omega$ and $\dot{\varepsilon}_{\mathrm{p}}^{\mathrm{vp}}=\dot{\gamma}^{\mathrm{vp}}\partial_{q_{\mathrm{p}}^{\mathrm{vp}}}\Omega$, which, in view of Eq. (43), are specifically expressed as, respectively,

$$\boldsymbol{l}^{\mathrm{vp}}=\dot{\gamma}^{\mathrm{vp}}\partial_{\boldsymbol{M}^{\mathrm{eff}}}\Sigma_{\mathrm{dev}}^{\mathrm{eq}},\ \dot{\varepsilon}^{\mathrm{vp}}=\dot{\gamma}^{\mathrm{vp}} \text{ and } \dot{\varepsilon}_{\mathrm{p}}^{\mathrm{vp}}=\dot{\gamma}^{\mathrm{vp}}\frac{q_{\mathrm{p}}^{\mathrm{vp}}}{s_{\mathrm{ss}}(T)}. \tag{44}$$

We also define the yield function as

$$f\left(\tau^{\mathrm{vol}},\boldsymbol{M}^{\mathrm{eff}},q^{\mathrm{vp}},T\right)=\alpha(T)\tau^{\mathrm{vol}}+\Sigma_{\mathrm{dev}}^{\mathrm{eq}}\left(\boldsymbol{M}^{\mathrm{eff}}\right)+q^{\mathrm{vp}}, \tag{45}$$

where $\alpha(T)$ is the pressure coefficient (Boyce et al., 1988a). Then, by substituting Eqns. (44) and (45) into Eqn. (8) and by considering $\Sigma_{\mathrm{dev}}^{\mathrm{eq}}=\boldsymbol{M}^{\mathrm{eff}}:\partial_{\boldsymbol{M}^{\mathrm{eff}}}\Sigma_{\mathrm{dev}}^{\mathrm{eq}}$ and $\Pi(f(\boldsymbol{Y}),\Lambda(\dot{\gamma}^{\mathrm{vp}}))=0$, we obtain the specific form of energy dissipation as

$$D^{\mathrm{eff}}=\dot{\gamma}^{\mathrm{vp}}\left\{-\alpha(T)\tau^{\mathrm{vol}}+\Lambda(\dot{\gamma}^{\mathrm{vp}})+\frac{\left(q_{\mathrm{p}}^{\mathrm{vp}}\right)^{2}}{s_{\mathrm{ss}}(T)}\right\}+\boldsymbol{G}\cdot\boldsymbol{Q}. \tag{46}$$

Here, if $D^{\mathrm{h}}=\boldsymbol{G}\cdot\boldsymbol{Q}\geq 0$ and $s_{\mathrm{Y}}^{0}(T)\geqslant\alpha(T)\tau^{\mathrm{vol}}$ are assumed to hold, the second law of thermodynamics is satisfied. Also, under the isothermal condition, the material time derivative of Eq. $(19)_2$ with Eqs. (4) and $(44)_2$ yields the following evolution equation of the shear yield strength:

$$\underbrace{\dot{q}_{\mathrm{p}}^{\mathrm{vp}} = h(T)\left(\dot{\bar{\varepsilon}}^{\mathrm{vp}} - \dot{\bar{\varepsilon}}_{\mathrm{p}}^{\mathrm{vp}}\right)}_{\text{Material time derivative of Eq. (19)}_2} = \underbrace{h(T)\left(\dot{\gamma}^{\mathrm{vp}} - \dot{\gamma}^{\mathrm{vp}}\frac{q_{\mathrm{p}}^{\mathrm{vp}}}{s_{\mathrm{ss}}(T)}\right)}_{\text{Substitution of Eq. (44)}}$$
$$= h(T)\left(1 - \frac{q_{\mathrm{p}}^{\mathrm{vp}}}{s_{\mathrm{ss}}(T)}\right)\dot{\gamma}^{\mathrm{vp}}, \text{ and } q_{\mathrm{p}}^{\mathrm{vp}}\Big|_{\text{pre-yield}} = s_{\mathrm{Y}}^{0}(T) \text{ from Eq. (19)}. \tag{47}$$

which is identical to that of Boyce et al. (1988a). This format itself can be implemented into fully coupled thermo-mechanical analyses. Nevertheless, our framework does not necessitate the material time derivative of $q_{\mathrm{p}}^{\mathrm{vp}}$ and hence not restricted to isothermal case; that is, the time variation of temperature in terms of material properties $h(T), s_{\mathrm{Y}}^{0}(T), s_{\mathrm{ss}}(T)$ can be taken into account.

On the other hand, introducing the evolution equation of the viscoplastic multiplier proposed by Richeton et al. (2005), we define the over stress as

$$\Lambda(\dot{\gamma}^{\mathrm{vp}}, T) = \bar{\sigma}_D(T)\sinh^{-1}\left[\left\{\eta^{\mathrm{vp}}(T)\left(\frac{\dot{\gamma}^{\mathrm{vp}}}{\dot{\gamma}_0^{\mathrm{vp}}}\right)\right\}^{\frac{1}{m}}\right], \tag{48}$$

where $\dot{\gamma}_0^{\mathrm{vp}}$ and m are the initial viscoplastic multiplier and real-valued material parameter, respectively. Also, $\bar{\sigma}_D$ and $\eta^{\mathrm{vp}}(T)$ are the drag stress and penalty parameter defined as, respectively,

$$\bar{\sigma}_D(T) = \frac{kT}{A} \text{ and } \eta^{\mathrm{vp}}(T) = \exp\left(\frac{\Delta H}{RT}\right), \tag{49}$$

where $\Delta H, A, R$ and k are the activation energy, activation volume, gas constant and Boltzmann constant, respectively. Finally, from Eq. (42), the dual viscoplastic dissipation potential $\tilde{\varphi}^{\mathrm{vp}}(\dot{\gamma}^{\mathrm{vp}}, T; \boldsymbol{F}, q_{\mathrm{p}}^{\mathrm{vp}})$ is derived as

$$\tilde{\varphi}^{\mathrm{vp}}\left(\dot{\gamma}^{\mathrm{vp}}, T; \boldsymbol{F}, q_{\mathrm{p}}^{\mathrm{vp}}\right) = \left\{-\alpha(T)\tau^{\mathrm{vol}} + \frac{\left(q_{\mathrm{p}}^{\mathrm{vp}}\right)^2}{s_{\mathrm{ss}}(T)}\right\}\dot{\gamma}^{\mathrm{vp}} + \int_0^{\dot{\gamma}^{\mathrm{vp}}} \Lambda\left(\hat{\dot{\gamma}}^{\mathrm{vp}}, T\right) d\hat{\dot{\gamma}}^{\mathrm{vp}}. \tag{50}$$

Remark 3. To realize the variational constitutive update, Farias et al. (2019) defined the function form of the shear yield strength with reference to the solution of Eq. (47). However, the approach is not versatile, since the material parameters in the evolution equation depend on the time-varying temperature.

4. Incremental variational framework

This section is devoted to formulating the thermo-mechanically coupled problem with non-associative viscoplasticity for glassy amorphous polymers within the incremental variational framework.

4.1. Outline

We outline the variational formulation for thermo-mechanically coupled problems, which is originally proposed by Yang et al. (2005) and further elaborated by Canadija and Mosler (2011).

The global energy rate ϕ is defined as

$$\phi\left(\dot{\boldsymbol{\varphi}}, T, \dot{\eta}, \dot{\boldsymbol{Z}}\right) \equiv \int_{B_0} \Upsilon\left(\dot{\boldsymbol{F}}, T, \dot{\eta}, \dot{\boldsymbol{Z}}\right) dV - G(\dot{\boldsymbol{\varphi}}, T), \tag{51}$$

with the following Dirichlet conditions on $\partial_{\mathrm{MD}}B_0$ and $\partial_{\mathrm{HD}}B_0$, respectively:

$$\dot{\boldsymbol{\varphi}} = \dot{\boldsymbol{\varphi}}_D \text{ on } \partial_{\mathrm{MD}}B_0 = \partial B_0 \setminus \partial_{\mathrm{MN}}B_0, T = T_D \text{ on } \partial_{\mathrm{HD}}B_0 = \partial B_0 \setminus (\partial_{\mathrm{HN}}B_0 \cup \partial_{\mathrm{HR}}B_0). \tag{52}$$

Here, $\partial_{\mathrm{MN}}B_0$ and $\partial_{\mathrm{HN}}B_0$ are the Neumann boundaries for the velocity and temperature fields, while the Robin condition is considered for heat transfer on boundary $\partial_{\mathrm{HR}}B_0$. Also, $G(\dot{\boldsymbol{\varphi}}, T)$ is the external power defined as

$$G(\dot{\boldsymbol{\varphi}}, T) = \int_{B_0} \rho_0 \boldsymbol{b}\cdot\dot{\boldsymbol{\varphi}} dV + \int_{\partial_{\mathrm{MN}}B_0} \boldsymbol{T}_{\mathrm{N}}\cdot\dot{\boldsymbol{\varphi}} dA + \int_{\partial_{\mathrm{HN}}B_0} \boldsymbol{Q}_{\mathrm{N}} \ln\left(\frac{T}{T_0}\right) dA + \int_{\partial_{\mathrm{HR}}B_0} \beta \left[T - T_0 \ln\left(\tfrac{T}{T_0}\right)\right] dA - \int_{B_0} \rho_0 h \ln\left(\frac{T}{T_0}\right) dV, \tag{53}$$

with the body force $\boldsymbol{b}$, the traction force $\boldsymbol{T}_{\mathrm{N}}$, the boundary heat flux $\boldsymbol{Q}_{\mathrm{N}}$, the coefficient of heat transfer β and the external heat supply h. In addition, Υ is the local energy rate defined as

$$\Upsilon\left(\dot{\boldsymbol{F}}, T, \dot{\eta}, \dot{\boldsymbol{Z}}\right) \equiv \rho_0 \dot{e}\left(\dot{\boldsymbol{F}}, \dot{\eta}, \dot{\boldsymbol{Z}}\right) - \rho_0 T\dot{\eta} + \varphi\left(\mathscr{F}(T,\theta)\dot{\boldsymbol{Z}}, \theta\right) - \chi(\boldsymbol{G}), \tag{54}$$

where $\dot{e}$ is the time rate of change of the internal energy and $\chi(\boldsymbol{G})$ is the Fourier potential given as

$$\chi(\boldsymbol{G}) = \frac{\kappa}{2}\boldsymbol{G}\cdot\boldsymbol{G} \geqslant 0, \tag{55}$$

with the material property for heat conduction κ. Here, $\mathscr{F}(T,\theta)$ is the integration factor defined as (Canadija and Mosler, 2011; Yang et al., 2005; Stainier and Ortiz, 2010)

$$\mathscr{F}(T,\theta) = \frac{T}{\theta}, \tag{56}$$

by which the variational structure of the thermo-mechanically coupled problem is ensured. Here, the "*equilibrium*" temperature $\theta \in \mathbb{R}_+$ is uniquely defined as $\theta = \partial_\eta(\rho_0 e)$, while the absolute temperature T, can be renamed to the "*external*" temperature, is an unknown variable. Then, the set of state variables $\left(\dot{\boldsymbol{\varphi}}^{\mathrm{opt}}, T^{\mathrm{opt}}, \dot{\eta}^{\mathrm{opt}}, \dot{\boldsymbol{Z}}^{\mathrm{opt}}\right)$ determining the instantaneous thermo-mechanically coupled stationary state is the solution of the following optimization problem for ϕ:

$$\left(\dot{\boldsymbol{\varphi}}^{\mathrm{opt}}, T^{\mathrm{opt}}, \dot{\eta}^{\mathrm{opt}}, \dot{\boldsymbol{Z}}^{\mathrm{opt}}\right) = \arg\left[\inf_{\dot{\boldsymbol{\varphi}}, \dot{\eta}, \dot{\boldsymbol{Z}}} \sup_{T} \phi\right] = \arg\left[\inf_{\dot{\boldsymbol{\varphi}}} \sup_{T} \phi\left(\inf_{\dot{\eta}, \dot{\boldsymbol{Z}}} \Upsilon\right)\right], \tag{57}$$

in which the infimum problem has been decomposed into the local and global ones, because $\dot{\eta}$ and $\dot{\boldsymbol{Z}}$ are confined to a material point.

Even though the framework just described above seems to be sufficient, the flow rule has not been considered yet. In this regard, in line with Mosler and Bruhns (2010), we parameterize the flow rule as

$$\dot{\boldsymbol{Z}}\left(\dot{\gamma}^{\mathrm{vp}}, \tilde{\boldsymbol{Y}}\right) = \dot{\gamma}^{\mathrm{vp}}\boldsymbol{N}\left(\tilde{\boldsymbol{Y}}\right), \tag{58}$$

where $\tilde{\boldsymbol{Y}}$ is called the 'pseudo' stress. It should be noted that the optimal $\tilde{\boldsymbol{Y}}^{\mathrm{opt}}$ determines the flow direction such that $\boldsymbol{N}\left(\tilde{\boldsymbol{Y}}\right) = \boldsymbol{N}(\boldsymbol{Y})$. This parameterization enables us to accomplish the variationally consistent formulation involving constraints on $\dot{\boldsymbol{Z}}$, which are associated with not only the yield function, but also plastic potential. Thus, the present framework accommodates even

non-associative flow rules; see References Mosler and Bruhns, 2008; Mosler, 2010 for the discussions in the same light. Accordingly, the global and local energy rates are rewritten as, respectively,

$$\phi\left(\dot{\boldsymbol{\varphi}},T,\dot{\eta},\dot{\gamma}^{\mathrm{vp}},\tilde{\boldsymbol{Y}}\right)=\int_{B_0}\Upsilon\left(\dot{\boldsymbol{F}},T,\dot{\eta},\dot{\gamma}^{\mathrm{vp}},\tilde{\boldsymbol{Y}}\right)dV-G(\dot{\boldsymbol{\varphi}},T) \tag{59}$$

$$\begin{aligned}\text{with}\quad \Upsilon\left(\dot{\boldsymbol{F}},T,\dot{\eta},\dot{\gamma}^{\mathrm{vp}},\tilde{\boldsymbol{Y}}\right)&=\rho_0\dot{e}\left(\dot{\boldsymbol{F}},\dot{\eta},\dot{\gamma}^{\mathrm{vp}},\tilde{\boldsymbol{Y}}\right)-\rho_0T\dot{\eta}\\&\quad+\varphi\left(\frac{T}{\theta}\dot{\gamma}^{\mathrm{vp}},\tilde{\boldsymbol{Y}},\theta\right)-\chi(\boldsymbol{G}),\end{aligned} \tag{60}$$

and the corresponding optimal state variables are given as

$$\begin{aligned}\left(\dot{\boldsymbol{\varphi}}^{\mathrm{opt}},T^{\mathrm{opt}},\dot{\eta}^{\mathrm{opt}},\dot{\gamma}^{\mathrm{vp,opt}},\tilde{\boldsymbol{Y}}^{\mathrm{opt}}\right)&=\arg\left[\inf_{\dot{\boldsymbol{\varphi}},\dot{\eta},\dot{\gamma}^{\mathrm{vp}},\tilde{\boldsymbol{Y}}}\sup_{T}\phi\right]\\&=\arg\left[\inf_{\dot{\boldsymbol{\varphi}}}\sup_{T}\phi\left(\inf_{\dot{\eta},\dot{\gamma}^{\mathrm{vp}},\tilde{\boldsymbol{Y}}}\Upsilon\right)\right].\end{aligned} \tag{61}$$

4.2. Stationary conditions

Now, we incorporate our constitutive model into the variational problem formulated above and establish that its stationary conditions reproduce the governing equations for the thermo-mechanically coupled problem; i.e., the variational consistency is guaranteed.

According to Eq. (44), the parameterized flow rules are expressed as

$$\boldsymbol{l}^{\mathrm{vp}}=\dot{\gamma}^{\mathrm{vp}}\partial_{\tilde{\boldsymbol{M}}^{\mathrm{eff}}}\Sigma^{\mathrm{eq}}_{\mathrm{dev}},\ \dot{\varepsilon}^{\mathrm{vp}}=\dot{\gamma}^{\mathrm{vp}}\ \text{and}\ \dot{\varepsilon}^{\mathrm{vp}}_{\mathrm{p}}=\dot{\gamma}^{\mathrm{vp}}\frac{q^{\mathrm{vp}}_{\mathrm{p}}}{s_{\mathrm{ss}}(\theta)}, \tag{62}$$

in which $\tilde{\boldsymbol{M}}^{\mathrm{eff}}$ is only the pseudo stress. It should be noted that the constraint $\dot{\lambda}^{\mathrm{vp}}=\dot{\gamma}^{\mathrm{vp}}$ has already been reflected in Eq. (62). Then, the substitution of Eq. (50) into Eq. (60) yields

$$\begin{aligned}&\Upsilon\left(\dot{\boldsymbol{F}},T,\dot{\eta},\dot{\gamma}^{\mathrm{vp}},\tilde{\boldsymbol{M}}^{\mathrm{eff}}\right)=\rho_0\dot{e}\left(\dot{\boldsymbol{F}},\dot{\eta},\dot{\gamma}^{\mathrm{vp}},\tilde{\boldsymbol{M}}^{\mathrm{eff}}\right)\\&-\rho_0T\dot{\eta}+\left(\frac{T}{\theta}\right)\left\{-\alpha(\theta)\tau^{\mathrm{vol}}+\frac{\left(q^{\mathrm{vp}}_{\mathrm{p}}\right)^2}{s_{\mathrm{ss}}(\theta)}\right\}\dot{\gamma}^{\mathrm{vp}}\\&+\left(\frac{T}{\theta}\right)\int_0^{\dot{\gamma}^{\mathrm{vp}}}\Lambda\left(\frac{T}{\theta}\hat{\dot{\gamma}}^{\mathrm{vp}};\theta\right)d\hat{\dot{\gamma}}^{\mathrm{vp}}-\chi(\boldsymbol{G}).\end{aligned} \tag{63}$$

Thus, the corresponding optimal state variables are solutions of the following optimization problem:

$$\left(\dot{\boldsymbol{\varphi}}^{\mathrm{opt}},T^{\mathrm{opt}},\dot{\eta}^{\mathrm{opt}},\dot{\gamma}^{\mathrm{vp,opt}},\tilde{\boldsymbol{M}}^{\mathrm{eff,opt}}\right)=\arg\left[\inf_{\dot{\boldsymbol{\varphi}}}\sup_{T}\phi\left(\inf_{\dot{\eta},\dot{\gamma}^{\mathrm{vp}},\tilde{\boldsymbol{M}}^{\mathrm{eff}}}\Upsilon\right)\right]. \tag{64}$$

First, the stationary conditions of Υ with respect to the local variations $\left(\delta\dot{\eta},\delta\dot{\gamma}^{\mathrm{vp}},\delta\tilde{\boldsymbol{M}}^{\mathrm{eff}}\right)$ are given as, respectively,

$$D\Upsilon[\delta\dot{\eta}]=\rho_0(\theta-T)\delta\dot{\eta}=0, \tag{65}$$

$$\begin{aligned}D\Upsilon[\delta\dot{\gamma}^{\mathrm{vp}}]=-\Big[&\left(\frac{T}{\theta}\right)\alpha(\theta)\tau^{\mathrm{vol}}+\boldsymbol{M}^{\mathrm{eff}}:\partial_{\tilde{\boldsymbol{M}}^{\mathrm{eff}}}\Sigma^{\mathrm{eq}}_{\mathrm{dev}}+q^{\mathrm{vp}}\\&-\left(\frac{T}{\theta}\right)\Lambda\left(\frac{T}{\theta}\dot{\gamma}^{\mathrm{vp}};\theta\right)+\left(1-\frac{T}{\theta}\right)\frac{\left(q^{\mathrm{vp}}_{\mathrm{p}}\right)^2}{s_{\mathrm{ss}}(\theta)}\Big]\delta\dot{\gamma}^{\mathrm{vp}}=0,\end{aligned} \tag{66}$$

$$D\Upsilon\left[\delta\tilde{\boldsymbol{M}}^{\mathrm{eff}}\right]=\dot{\gamma}^{\mathrm{vp}}\boldsymbol{M}^{\mathrm{eff}}:\partial^2_{\tilde{\boldsymbol{M}}^{\mathrm{eff}}\tilde{\boldsymbol{M}}^{\mathrm{eff}}}\Sigma^{\mathrm{eq}}_{\mathrm{dev}}:\delta\tilde{\boldsymbol{M}}^{\mathrm{eff}}=0. \tag{67}$$

Here, Eq. (65) implies the thermodynamical equilibrium state such that $\theta=T$, while Eq. (67) reproduces the homogeneity of $\Sigma^{\mathrm{eq}}_{\mathrm{dev}}$. With θ substituting for T and the yield function in Eq. (45) being considered, Eq. (66) is rewritten as

$$D\Upsilon[\delta\dot{\gamma}^{\mathrm{vp}}]=-\left\{f\left(\boldsymbol{M}^{\mathrm{eff}},q^{\mathrm{vp}},\theta\right)-\Lambda(\dot{\gamma}^{\mathrm{vp}};\theta)\right\}\delta\dot{\gamma}^{\mathrm{vp}}=0. \tag{68}$$

Thus, the stationary condition of Υ with respect to $\dot{\gamma}^{\mathrm{vp}}$ is identical to the extended yield criterion $\Pi(f(\boldsymbol{Y},\theta),\Lambda(\dot{\gamma}^{\mathrm{vp}},\theta))=0$ provided in Eq. (30).

Next, the Gateaux derivatives of the locally optimized energy rate $\Upsilon^{\mathrm{opt}}=\inf_{\dot{\eta},\dot{\gamma}^{\mathrm{vp}},\tilde{\boldsymbol{M}}^{\mathrm{eff}}}\Upsilon$ with respect to the global variations $(\delta\dot{\boldsymbol{\varphi}},\delta T)$ are given as, respectively,

$$D\Upsilon^{\mathrm{opt}}[\delta\dot{\boldsymbol{\varphi}}]=\boldsymbol{P}:\nabla_{\boldsymbol{X}}\delta\dot{\boldsymbol{\varphi}}, \tag{69}$$

$$\begin{aligned}D\Upsilon^{\mathrm{opt}}[\delta T]=&-\rho_0\dot{\eta}\delta T+\left(\frac{\delta T}{\theta}\right)\left\{-\alpha(\theta)\tau^{\mathrm{vol}}+\frac{\left(q^{\mathrm{vp}}_{\mathrm{p}}\right)^2}{s_{\mathrm{ss}}(\theta)}\right\}\dot{\gamma}^{\mathrm{vp}}\\&+\partial_T\left\{\frac{T}{\theta}\int_0^{\dot{\gamma}^{\mathrm{vp}}}\Lambda\left(\frac{T}{\theta}\hat{\dot{\gamma}}^{\mathrm{vp}};\theta\right)d\hat{\dot{\gamma}}^{\mathrm{vp}}\right\}\delta T+\boldsymbol{Q}\cdot\nabla_{\boldsymbol{X}}\left(\frac{\delta T}{T}\right),\end{aligned} \tag{70}$$

where the third term in the right-hand side of Eq. (70) is expressed as

$$\begin{aligned}&\partial_T\left\{\frac{T}{\theta}\int_0^{\dot{\gamma}^{\mathrm{vp}}}\Lambda\left(\frac{T}{\theta}\hat{\dot{\gamma}}^{\mathrm{vp}};\theta\right)d\hat{\dot{\gamma}}^{\mathrm{vp}}\right\}=\frac{1}{\theta}\int_0^{\dot{\gamma}^{\mathrm{vp}}}\Lambda\left(\frac{T}{\theta}\hat{\dot{\gamma}}^{\mathrm{vp}};\theta\right)d\hat{\dot{\gamma}}^{\mathrm{vp}}\\&+\frac{T}{\theta}\int_0^{\dot{\gamma}^{\mathrm{vp}}}\partial_T\Lambda\left(\frac{T}{\theta}\hat{\dot{\gamma}}^{\mathrm{vp}};\theta\right)d\hat{\dot{\gamma}}^{\mathrm{vp}}\end{aligned} \tag{71}$$

Therefore, the stationary conditions of ϕ with respect to the global variations $(\delta\dot{\boldsymbol{\varphi}},\delta T)$ are given as, respectively,

$$D\phi\left[\delta\dot{\boldsymbol{\varphi}}\right]=\int_{B_0}\boldsymbol{P}:\nabla_{\boldsymbol{X}}\delta\dot{\boldsymbol{\varphi}}dV-\int_{B_0}\rho_0\boldsymbol{b}\cdot\delta\dot{\boldsymbol{\varphi}}dV-\int_{\partial_{\mathrm{MN}}B_0}\boldsymbol{T}_{\mathrm{N}}\cdot\delta\dot{\boldsymbol{\varphi}}dA=0 \tag{72}$$

$$\begin{aligned}D\phi[\delta T]=&-\int_{B_0}\rho_0\dot{\eta}\delta TdV+\int_{B_0}\dot{\gamma}^{\mathrm{vp}}\left\{-\alpha(\theta)\tau^{\mathrm{vol}}+\frac{\left(q^{\mathrm{vp}}_{\mathrm{p}}\right)^2}{s_{\mathrm{ss}}(\theta)}\right\}\left(\frac{\delta T}{\theta}\right)dV\\&+\int_{B_0}\partial_T\left\{\frac{T}{\theta}\int_0^{\dot{\gamma}^{\mathrm{vp}}}\Lambda\left(\frac{T}{\theta}\hat{\dot{\gamma}}^{\mathrm{vp}};\theta\right)d\hat{\dot{\gamma}}^{\mathrm{vp}}\right\}\delta TdV+\int_{B_0}\boldsymbol{Q}\cdot\nabla_{\boldsymbol{X}}\left(\frac{\delta T}{T}\right)dV\\&-\int_{\partial_{\mathrm{HN}}B_0}\boldsymbol{Q}_N\frac{\delta T}{T}dA-\int_{\partial_{\mathrm{HR}}B_0}\beta\left[1-\frac{T_0}{T}\right]\delta TdA+\int_{B_0}\rho_0h\frac{\delta T}{T}dV=0.\end{aligned} \tag{73}$$

It is obvious that these are identified as the equations of virtual work rate in terms of the mechanical equilibrium and unsteady heat conduction, respectively.

4.3. Time discretization of the specialized problem

The global energy increment is obtained by the time integration of Eq. (51) over the time interval $[t_n,t_{n+1}]$ as

$$\begin{aligned}\Psi_{n+1}&=\inf_{\mathrm{path}}\int_{t_n}^{t_{n+1}}\phi\left(\dot{\boldsymbol{\varphi}},T,\dot{\eta},\dot{\gamma}^{\mathrm{vp}},\tilde{\boldsymbol{M}}^{\mathrm{eff}};\theta\right)dt\\&=\inf_{\mathrm{path}}\int_{t_n}^{t_{n+1}}\left[\int_{B_0}\Upsilon\left(\dot{\boldsymbol{F}},T,\dot{\eta},\dot{\gamma}^{\mathrm{vp}},\tilde{\boldsymbol{M}}^{\mathrm{eff}};\theta\right)dV-G(\dot{\boldsymbol{\varphi}},T)\right]dt\end{aligned} \tag{74}$$

which indicates that ϕ is constantly minimized along the equilibrium path. Applying the backward Euler approximation to all the time-varying variables in the integrand such that $\boldsymbol{\Xi}\approx(\boldsymbol{\Xi}_{n+1}-\boldsymbol{\Xi}_n)/\Delta t$ with Δt being the time increment, we obtain the time-discretized version of Eq. (74) as

$$\Psi_{n+1}=\int_{B_0}\Upsilon_{n+1}\left(\boldsymbol{F}_{n+1},T_{n+1},\Delta\gamma^{\mathrm{vp}}_{n+1},\tilde{\boldsymbol{M}}^{\mathrm{eff}}_{n+1}\right)dV-G_{n+1}\left(\boldsymbol{\varphi}_{n+1},T_{n+1}\right). \tag{75}$$

For the sake of simplicity, the internal energy rate has been replaced by the free energy rate, and thus the entropy is treated as an explicitly defined function depending on the external temperature; see Eqs. (24)–(26). Also, the parameterized flow rules are discretized in time as

$$\boldsymbol{F}^{\mathrm{vp}}_{n+1} = \exp\left(\Delta\gamma^{\mathrm{vp}}\partial_{\tilde{\boldsymbol{M}}^{\mathrm{eff}}_{n+1}}\Sigma^{\mathrm{eq}}_{\mathrm{dev},n+1}\right)\boldsymbol{F}^{\mathrm{vp}}_{n}, \tag{76}$$

$$\bar{\varepsilon}^{\mathrm{vp}}_{n+1} = \bar{\varepsilon}^{\mathrm{vp}}_{n} + \Delta\gamma^{\mathrm{vp}}, \tag{77}$$

$$\bar{\varepsilon}^{\mathrm{vp}}_{\mathrm{p},n+1} = \left(1 + h(T_n)\frac{\Delta\gamma^{\mathrm{vp}}}{s_{\mathrm{ss}}(T_n)}\right)^{-1}\times \left\{\bar{\varepsilon}^{\mathrm{vp}}_{\mathrm{p},n} + \frac{\Delta\gamma^{\mathrm{vp}}}{s_{\mathrm{ss}}(T_n)}\left(h(T_n)\bar{\varepsilon}^{\mathrm{vp}}_{n+1} + s^0_{\mathrm{Y}}(T_n)\right)\right\}, \tag{78}$$

$$\because\ q^{\mathrm{vp}}_{\mathrm{p},n+1} = h(T_n)\left(\bar{\varepsilon}^{\mathrm{vp}}_{n+1} - \bar{\varepsilon}^{\mathrm{vp}}_{\mathrm{p},n+1}\right) + s^0_{\mathrm{Y}}(T_n), \tag{79}$$

in which the equilibrium temperature has been approximated at T_n to avoid unnecessary complexity. Then, the local energy rate and the external power are discretized as, respectively,

$$\begin{aligned}
&\Upsilon_{n+1}\left(\boldsymbol{F}_{n+1}, T_{n+1}, \Delta\gamma^{\mathrm{vp}}, \tilde{\boldsymbol{M}}^{\mathrm{eff}}_{n+1}\right)\\
&= \rho_0\psi_{n+1}\left(\boldsymbol{F}_{n+1}, T_{n+1}, \Delta\gamma^{\mathrm{vp}}, \tilde{\boldsymbol{M}}^{\mathrm{eff}}_{n+1}\right)\\
&-\rho_0\psi_n + \rho_0(T_{n+1}-T_n)\eta_n\\
&+\left(\frac{T_{n+1}}{T_n}\right)\left\{-\alpha(T_n)\tau^{\mathrm{vol}}_{n+1} + \frac{\left(q^{\mathrm{vp}}_{\mathrm{p},n+1}\right)^2}{s_{\mathrm{ss}}(T_n)}\right\}\Delta\gamma^{\mathrm{vp}}\\
&+\left(\frac{T_{n+1}}{T_n}\right)\int_0^{\Delta\gamma^{\mathrm{vp}}}\Lambda_{n+1}\left(\frac{T_{n+1}}{T_n\Delta t}\Delta\hat{\gamma}^{\mathrm{vp}}, T_n\right)d\Delta\hat{\gamma}^{\mathrm{vp}} - \Delta t\chi_{n+1}(\boldsymbol{G}_{n+1}),
\end{aligned} \tag{80}$$

$$\begin{aligned}
&G_{n+1}(\boldsymbol{\varphi}_{n+1}, T_{n+1}) = \int_{B_0}\rho_0\boldsymbol{b}\cdot(\boldsymbol{\varphi}_{n+1}-\boldsymbol{\varphi}_n)dV\\
&+\int_{\partial_{\mathrm{MN}}B_0}\boldsymbol{T}_{\mathrm{N}}\cdot(\boldsymbol{\varphi}_{n+1}-\boldsymbol{\varphi}_n)dA\\
&-\int_{B_0}\Delta t\rho_0 h\ln\left(\frac{T_{n+1}}{T_0}\right)dV\\
&+\int_{\partial_{\mathrm{HN}}B_0}\Delta t\boldsymbol{Q}_{\mathrm{N}}\ln\left(\frac{T_{n+1}}{T_0}\right)dA\\
&;\quad +\int_{\partial_{\mathrm{HR}}B_0}\Delta t\beta\left[T_{n+1} - T_0\ln\left(\frac{T_{n+1}}{T_0}\right)\right]dA.
\end{aligned} \tag{81}$$

Thus, the set of optimized solutions is identified with

$$\left(\boldsymbol{\varphi}^{\mathrm{opt}}_{n+1}, T^{\mathrm{opt}}_{n+1}, \Delta\gamma^{\mathrm{vp,opt}}, \tilde{\boldsymbol{M}}^{\mathrm{eff,opt}}_{n+1}\right) = \arg\left[\inf_{\boldsymbol{\varphi}_{n+1}}\sup_{T_{n+1}}\Psi_{n+1}\left(\inf_{\Delta\gamma^{\mathrm{vp}},\tilde{\boldsymbol{M}}^{\mathrm{eff}}_{n+1}}\Upsilon_{n+1}\right)\right]. \tag{82}$$

This optimization problem can be solved with the standard Newton–Raphson method, the details of which is found in Bleier and Mosler (2012).

Fig. 1 summarizes the proposed incremental variational formulation of the thermo-mechanically coupled problem with the time-discretized variational constitutive equations for glassy amorphous polymers.

Remark 4. When the time discretization is coarse, the stationary conditions of Eq. (80) with respect to $\Delta\gamma^{\mathrm{vp}}$ and $\boldsymbol{F}_{n+1}$ are not consistent with Eq. (30) and the adopted hyperelastic constitutive equation, respectively; see Mosler and Bruhns (2008) and Mosler (2010) in this regard. However, if the time continuous case $\Delta t \to 0$ is considered, the variational consistency of the present formulation is exactly reproduced. It is, therefore, pertinent to properly set the time increment in actual computations.

5. Representative numerical example

This section is devoted to verifying the appropriateness of the proposed formulation. To this end, we adopted the set of compression tests for PMMA reported in Arruda et al. (1995) as a target problem.

5.1. Preparation

5.1.1. Material parameters

In order to perform thermo-mechanically coupled analyses by the proposed model, we need to determine the following material parameters in advance:

1. Elastic moduli and coefficient of thermal expansion: $K(T)$, $G(T)$, $\alpha_{\mathrm{th}}(T)$
2. Hardening parameters: $\alpha(T)$, $h(T)$, $s^0_{\mathrm{Y}}(T)$, $s_{\mathrm{ss}}(T)$, $\mu(T)$, $J_{\mathrm{m}}(T)$
3. Over stress parameters: A, ΔH, $\dot{\gamma}^{\mathrm{vp}}_0$, m
4. Thermal properties: ρ, c, κ

Among these, the parameters available in the literature are the following:

1. Elastic moduli (Arruda et al., 1995) and coefficient of thermal expansion (Boyce et al., 1988b):
$$K(T) = \frac{2G(T)(1+\nu)}{3(1-2\nu)}\,[\mathrm{MPa}],\ \ln G(T) = \ln(1205) - 0.00118(T-298)[\mathrm{MPa}],$$
$$\nu = 0.33,\ \alpha_{\mathrm{th}}(T) = 2.6\times10^{-4}(T-T_0)$$
2. Hardening parameters (Arruda et al., 1995):
$$\alpha(T) = 0.0867,\ \mu(T) = kT\left[B - D\exp\left(\frac{-E_a}{RT}\right)\right]\ [\mathrm{Pa}]$$
$$B = 2.95\times10^{27}\ [\mathrm{m}^{-3}],\ D = 1.28\times10^{31}\ [\mathrm{m}^{-3}],$$
$$E_a = 5.6\ [\mathrm{kcal}\cdot\mathrm{mol}^{-1}]$$
3. Activation energy (Richeton et al., 2007):
$$\Delta H = 90.0\,[\mathrm{kJ}\cdot\mathrm{mol}^{-1}]$$
4. Thermal properties (Arruda et al., 1995):
$$\rho = 1200\,[\mathrm{kg}\cdot\mathrm{m}^{-3}],\ c = 1460\,[\mathrm{J}\cdot\mathrm{kg}^{-1}\cdot\mathrm{K}^{-1}],$$
$$\kappa = 57.216\,[\mathrm{W}\cdot\mathrm{m}^{-1}]$$

The remaining parameters, $h(T)$, $s^0_{\mathrm{Y}}(T)$, $s_{\mathrm{ss}}(T)$, $J_{\mathrm{m}}(T)$, A, $\dot{\gamma}^{\mathrm{vp}}_0$ and m, are determined by curve fitting by reference to the relationships between true stresses and true strains that were measured in the uniaxial compression tests under the isothermal condition; readers are referred to the corresponding curves in Reference Arruda et al. (1995). Fig. 2 compares the curve-fitting results with the predicted curves and the experimental data in the previous research, and the identified material parameters are listed below.

1. Hardening parameters:
$$h(T) = 62.0\ [\mathrm{MPa}],$$
$$s^0_{\mathrm{Y}}(T) = 172.856 - 0.458T\ [\mathrm{MPa}]\ (\mathrm{Richeton\ et\ al.}[9]),$$
$$s_{\mathrm{ss}}(T) = 0.55s^0_{\mathrm{Y}}(T)[\mathrm{MPa}],\ J_{\mathrm{m}}(T) = 4.8 + 0.095(T-298)$$
2. Overstress parameters:
$$A = 4.605\times10^{-29}\,[\mathrm{m}^3],\ \dot{\gamma}^{\mathrm{vp}}_0 = 5.6\times10^{16}\,[\mathrm{s}^{-1}],\ m = 5.95$$

As can be seen from this figure, the overall responses represented by the material model employed in this study are in close agreement with those of the previous research. It seems, however, that the prediction accuracy of our curve fitting is slightly worse than that of the previous research especially within the range of true compressive strain of 0.6–1.2 in the case of 25.0 [deg]. This discrepancy is probably due to the adopted kinematic hardening models to represent the entropic resistance of amorphous polymers (Boyce, 1996). Indeed,

$$\text{Optimized solutions}: \quad \left(\boldsymbol{\varphi}_{n+1}^{\mathrm{opt}}, T_{n+1}^{\mathrm{opt}}, \Delta\gamma_{n+1}^{\mathrm{vp,opt}}, \tilde{\boldsymbol{M}}_{n+1}^{\mathrm{eff,opt}}\right) = \arg\left[\inf_{\boldsymbol{\varphi}_{n+1}, \Delta\gamma_{n+1}^{\mathrm{vp}}, \tilde{\boldsymbol{M}}_{n+1}^{\mathrm{eff}}} \sup_{T_{n+1}} \left\{\int_{B_0} \Upsilon_{n+1} dV - G_{n+1}\right\}\right]$$

$$\text{Local energy increment}: \quad \Upsilon_{n+1}\left(\boldsymbol{F}_{n+1}, T_{n+1}, \Delta\gamma_{n+1}^{\mathrm{vp}}, \tilde{\boldsymbol{M}}_{n+1}^{\mathrm{eff}}\right) = \rho_0\psi_{n+1} - \rho_0\psi_n + \rho_0\left(T_{n+1} - T_n\right)\eta_n + \tilde{\varphi}_{n+1}^{\mathrm{vp}} - \chi_{n+1}$$

— Helmholtz free energy : $\rho_0\psi_{n+1}\left(\boldsymbol{F}_{n+1}, T_{n+1}, \Delta\gamma_{n+1}^{\mathrm{vp}}, \tilde{\boldsymbol{M}}_{n+1}^{\mathrm{eff}}\right) = \rho_0\psi_{n+1}^{\mathrm{e}} + \rho_0\psi_{n+1}^{\mathrm{vp}} + \rho_0\psi_{n+1}^{\mathrm{h}}$

$$\rho_0\psi_{n+1}^{\mathrm{e}}\left(\boldsymbol{F}_{n+1}, T_{n+1}, \Delta\gamma_{n+1}^{\mathrm{vp}}, \tilde{\boldsymbol{M}}_{n+1}^{\mathrm{eff}}\right) = \underbrace{\frac{1}{2}K\left(T_{n+1}\right)\left(\ln J_{n+1}\right)^2 - 3K\left(T_{n+1}\right)\alpha_{\mathrm{th}}\left(T_{n+1}\right)\ln J_{n+1}}_{=\rho_0\psi_{\mathrm{vol},n+1}^{\mathrm{e}}} + \underbrace{G\left(T_{n+1}\right)\overline{\boldsymbol{\varepsilon}}_{\mathrm{H},n+1}^{\mathrm{e}} : \overline{\boldsymbol{\varepsilon}}_{\mathrm{H},n+1}^{\mathrm{e}}}_{=\rho_0\psi_{\mathrm{dev},n+1}^{\mathrm{e}}}$$

$$\rho_0\psi_{n+1}^{\mathrm{vp}}\left(T_{n+1}, \Delta\gamma_{n+1}^{\mathrm{vp}}, \tilde{\boldsymbol{M}}_{n+1}^{\mathrm{eff}}\right) = \underbrace{\frac{h\left(T_{n+1}\right)}{2}\left(\overline{\varepsilon}_{\mathrm{e},n+1}^{\mathrm{vp}}\right)^2 + s_{\mathrm{Y}}^0\left(T_{n+1}\right)\overline{\varepsilon}_{\mathrm{e},n+1}^{\mathrm{vp}}}_{=\rho_0\psi_{\mathrm{iso},n+1}^{\mathrm{vp}}} \underbrace{- \mu\left(T_{n+1}\right)J_{\mathrm{m}}\left(T_{n+1}\right)\ln\left(1 - \frac{\overline{I}_{1,n+1}^{\mathrm{vp}} - 3}{J_{\mathrm{m}}\left(T_{n+1}\right)}\right)}_{=\rho_0\psi_{\mathrm{kin},n+1}^{\mathrm{vp}}}$$

$$\rho_0\psi_{n+1}^{\mathrm{h}}\left(T_{n+1}\right) = \rho_0 c\left\{T_{n+1} - T_0 - T_{n+1}\ln\left(\frac{T_{n+1}}{T_0}\right)\right\}$$

— Dual viscoplastic dissipation potential :

$$\tilde{\varphi}_{n+1}^{\mathrm{vp}}\left(\boldsymbol{F}_{n+1}, T_{n+1}, \Delta\gamma_{n+1}^{\mathrm{vp}}\right) = \left(\frac{T_{n+1}}{T_n}\right)\left\{-\alpha\left(T_n\right)\tau_{n+1}^{\mathrm{vol}}\left(\boldsymbol{F}_{n+1}\right) + \frac{\left(q_{\mathrm{p},n+1}^{\mathrm{vp}}\right)^2}{s_{\mathrm{ss}}\left(T_n\right)}\right\}\Delta\gamma_{n+1}^{\mathrm{vp}} + \underbrace{\frac{T_{n+1}}{T_n}\int_0^{\Delta\gamma_{n+1}^{\mathrm{vp}}} \overline{\sigma}_{\mathrm{D}}\left(T_n\right)\sinh^{-1}\left[\left\{\eta^{\mathrm{vp}}\left(T_n\right)\left(\frac{T_{n+1}\Delta\hat{\gamma}^{\mathrm{vp}}}{T_n\Delta t\dot{\gamma}_0^{\mathrm{vp}}}\right)\right\}^{\frac{1}{m}}\right] d\Delta\hat{\gamma}^{\mathrm{vp}}}_{=\Lambda_{n+1}}$$

— Fourier potential : $\chi_{n+1}\left(T_{n+1}\right) = \dfrac{\kappa\Delta t}{2}\boldsymbol{G}_{n+1}\cdot\boldsymbol{G}_{n+1}$

$$\text{External work increment}: \quad G_{n+1}\left(\boldsymbol{\varphi}_{n+1}, T_{n+1}\right) = \int_{B_0}\rho_0\boldsymbol{b}\cdot\left(\boldsymbol{\varphi}_{n+1} - \boldsymbol{\varphi}_n\right)dV + \int_{\partial_{\mathrm{MN}}B_0}\boldsymbol{T}_{\mathrm{N}}\cdot\left(\boldsymbol{\varphi}_{n+1} - \boldsymbol{\varphi}_n\right)dA$$
$$+ \int_{\partial_{\mathrm{HN}}B_0}\Delta t\boldsymbol{Q}_{\mathrm{N}}\ln\left(\frac{T_{n+1}}{T_0}\right)dA + \int_{\partial_{\mathrm{HR}}B_0}\Delta t\beta\left[T_{n+1} - T_0\ln\left(\frac{T_{n+1}}{T_0}\right)\right]dA - \int_{B_0}\Delta t\rho_0 h\ln\left(\frac{T_{n+1}}{T_0}\right)dV$$

$$\text{With parameterized flow rule}: \quad \begin{cases} \boldsymbol{F}_{n+1}^{\mathrm{vp}} = \exp\left(\Delta\gamma_{n+1}^{\mathrm{vp}}\partial_{\tilde{\boldsymbol{M}}_{n+1}^{\mathrm{eff}}}\Sigma_{\mathrm{dev},n+1}^{\mathrm{eq}}\right)\boldsymbol{F}_n^{\mathrm{vp}} \\ \overline{\varepsilon}_{n+1}^{\mathrm{vp}} = \overline{\varepsilon}_n^{\mathrm{vp}} + \Delta\gamma_{n+1}^{\mathrm{vp}} \\ \overline{\varepsilon}_{\mathrm{p},n+1}^{\mathrm{vp}} = \left(1 + h\left(T_n\right)\dfrac{\Delta\gamma_{n+1}^{\mathrm{vp}}}{s_{\mathrm{ss}}\left(T_n\right)}\right)^{-1}\left\{\overline{\varepsilon}_{\mathrm{p},n}^{\mathrm{vp}} + \dfrac{\Delta\gamma_{n+1}^{\mathrm{vp}}}{s_{\mathrm{ss}}\left(T_n\right)}\left(h\left(T_n\right)\overline{\varepsilon}_{n+1}^{\mathrm{vp}} + s_{\mathrm{Y}}^0\left(T_n\right)\right)\right\} \end{cases}$$

Fig. 1. Summary of proposed incremental variational formulation of thermo-mechanically coupled problems with time-discretized variational constitutive equations for glassy amorphous polymers.

Arruda-Boyce model (Arruda and Boyce, 1993a,b) seems to be more suitable for the material under consideration than Gent model (Gent, 1996) employed in this study. Nevertheless, as argued in Remark 2, Arruda-Boyce model, strictly speaking, is not applicable to variationally consistent formulations for thermo-mechanically coupled problems, because the entropy has a non-zero value under the isothermal and no-load conditions. For this reason, the present model with the identified material parameters is acceptable to carry out the thermo-mechanically coupled analyses for the purpose of verification of the proposed formulation.

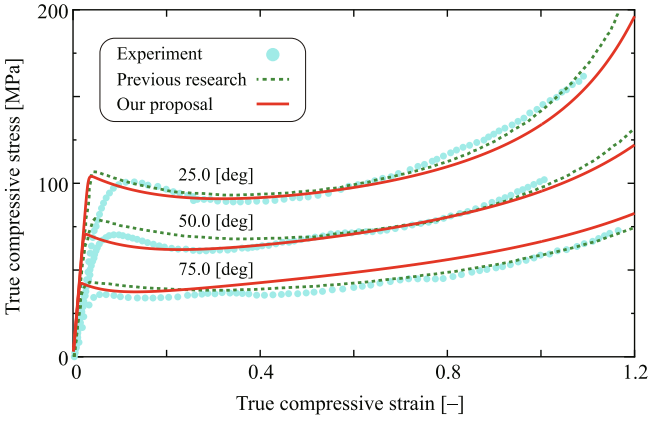

Fig. 2. Fitted curves with identified parameters and predicted curves in the Arruda et al. (1995) in comparison with experiment data.

Meanwhile, the rate-dependent responses of the material model are also confirmed in the left side of Fig. 3 that shows the relationships between true compressive stresses and true compressive strains for three different levels of strain rate under the isothermal and adiabatic conditions with the initial temperature of 25.0 [deg]. Here, the compression test under the adiabatic condition has been simulated through the fully coupled thermo-mechanical analysis with one twenty-node hexahedral element, for which all degrees of freedom (DOFs) associated with temperature are set to be free. The right side of this figure shows the relationship between the temperature and true compressive strain in

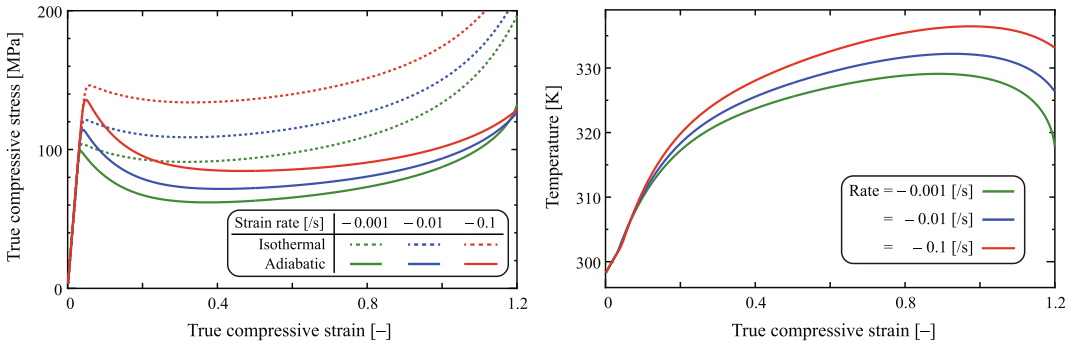

Fig. 3. Constitutive responses under isothermal and adiabatic conditions with an initial temperature of 25.0 [deg]. [Left side]: Relationships between true compressive stresses and true compressive strains for three levels of strain rates; dotted and solid lines correspond to isothermal and adiabatic cases, respectively. [Right side]: Relationships between temperatures and true compressive strains for adiabatic state.

the adiabatic case. As can be seen from the former, each of the true compressive stresses in the adiabatic case attains the local maximum in a relatively small strain range and is slightly smaller than that of the isothermal case for every level of strain rate. The reason is that the temperature elevation due to the elastic entropy change makes the yield stress decrease. Also, the post-yield stresses are drastically decreased, even though the pre-yield stresses are close to those in the isothermal case. This must also be due to the strain softening and stiffness reduction caused by the temperature elevation, the maximum of which reaches over 330 [K] as can be seen from the right side of the figure. Further, the rate dependency of temperature elevation is observed because the overstress inducing the self-generated heat increases with the increase of viscoplastic multiplier.

Once the true compressive strain exceeds about 0.8, the evolution of viscoplastic deformation is suppressed by the back stress elevation associated with the entropic resistance and, as a result, the self-generated heat becomes smaller. At the same time, the corresponding entropy represented by Eq. (25) drastically increases under the influence of the limiting chain extensibility and causes local heat absorption. In fact, as can be seen in Fig. 4 depicted in Arruda et al. (1995), the decrease in temperature can be experimentally observed even for the almost adiabatic state. Thus, we are convinced that the entropy resulting from orientation hardening makes the temperature in the specimen decrease. For this reason, the non-negligible temperature reduction occurs despite keeping the adiabatic state.

5.1.2. Finite element model and analysis condition

A cubic PMMA specimen attached to the testing machine is targeted and its schematic view is shown in Fig. 4(a). One-eighth of the entire structure is discretized with twenty-node (2nd order) hexahedral elements as shown in Fig. 4(b), whereas the axisymmetric model is adopted in Reference Arruda et al. (1995). For both the thermal and mechanical problems, the symmetry conditions is applied to –XY, –XZ and –YZ planes indicated in the Fig. 4(a). The same amount of enforced displacement is given at a constant true strain rate to the Z-components of all the nodal displacement vectors of the FE model of the steel attachment, while the other components are set to be free from constraints. The total number of calculation steps is set to be 1,000. It has been confirmed that when a much larger number of calculation steps is set, the solution showed little change.

Although the testing machine is made of steel, only a negligibly small stiffness is virtually assigned to the steel so that it can deform in the in-plane direction without any mechanical resistance. This setting is intended to realize a uniaxial compression state of the specimen and uniform stress distribution without the consideration of contact conditions and friction effects as much as possible. To see the rate-dependency of the structural responses, three different true strain rates are considered; $\dot{\varepsilon}^{z}_{H} = -0.001, -0.01, -0.1\ \left[\mathrm{s}^{-1}\right]$.

Meanwhile, the steel is given actual thermal properties so as to be an actual medium only for the thermal problem. To this end, the thermal properties of the steel are set at

$$\rho^{s} = 7870\ \left[\mathrm{kg}\cdot\mathrm{m}^{-3}\right],\ c^{s} = 442\ \left[\mathrm{J}\cdot\mathrm{kg}^{-1}\cdot\mathrm{K}^{-1}\right],$$
$$\kappa^{s} = 24090\ \left[\mathrm{W}\cdot\mathrm{m}^{-1}\right].$$

Also, the heat transfer condition is applied to the external surfaces of the model and the heat transfer coefficient is set at $\beta = 85.0\ \left[\mathrm{W}\cdot\mathrm{m}^{-2}\cdot\mathrm{K}^{-1}\right]$ commonly for both the materials for the sake of simplicity. The initial and ambient temperatures are set at 22.0 [deg] and the latter is assumed to be unchanged throughout the numerical analysis.

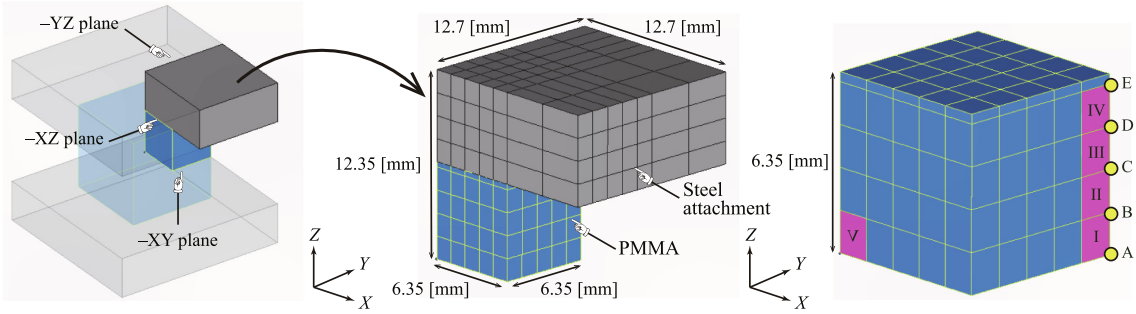

(a) Specimen attached to the testing machine (b) One-eighth model of the entire structure (c) Specimen model with tracing nodes and elements

Fig. 4. Specimen attached to a steel-made testing machine and one-eighth FE model with selected nodes and elements for tracing (Arruda et al., 1995).

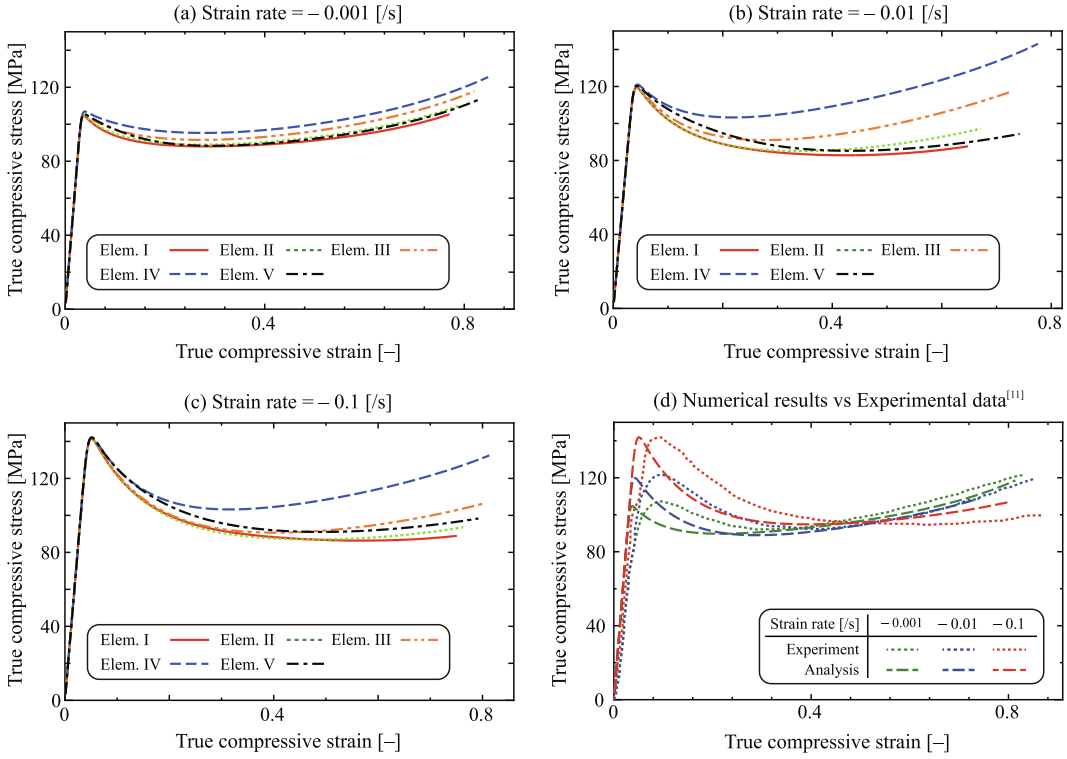

Fig. 5. Relationships between true compressive stresses and true compressive strains in five selected elements for three levels of true strain rates.

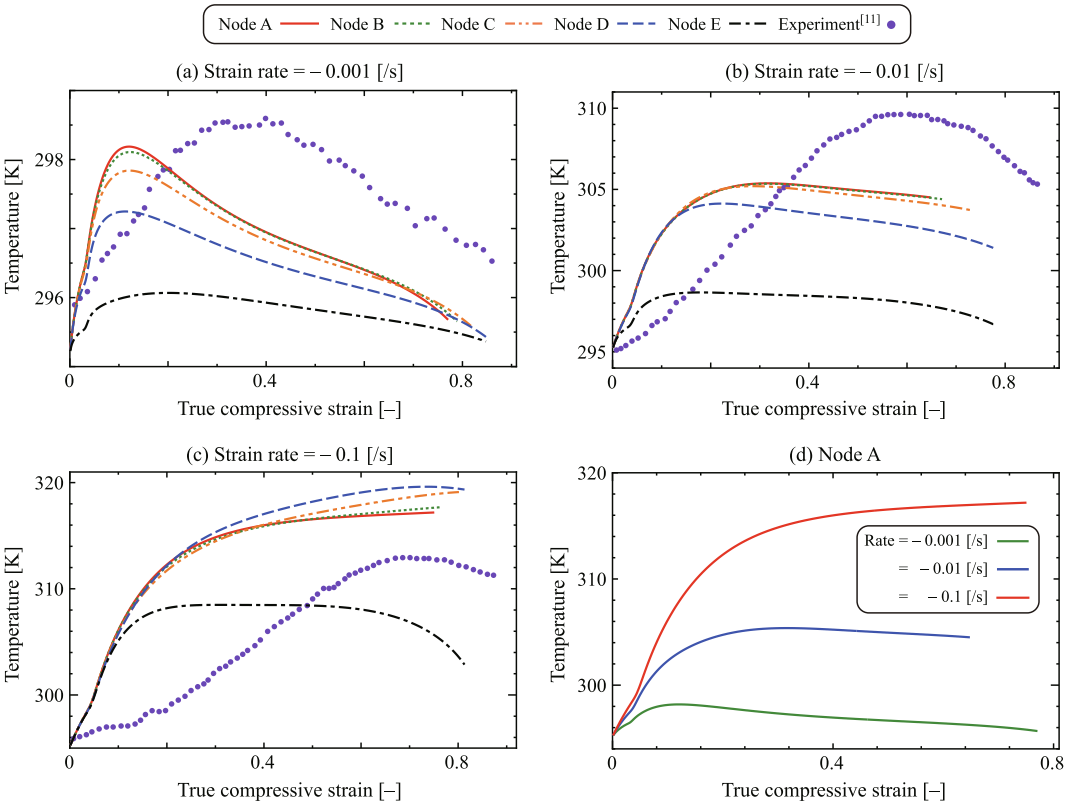

Fig. 6. Relationships between temperatures and true compressive strains at five selected nodes for three levels of true strain rates.

5.2. Results and discussion

To illustrate the predicted thermo-mechanical behavior, we have traced both the sets of true compressive stresses and strains calculated in the five purple-colored elements and the temperatures measured at the five nodes indicated by yellow markers indicated in Fig. 4(c). Fig. 5 shows the relationship between the true compressive stress and true compressive strain in response to each strain rate. Here, the true compressive stresses in Fig. 5(d) are evaluated by dividing the reaction force by the current area on the upper surface of the specimen, while the true compressive strains are the apparent strains calculated by the height change of the specimen: $\tilde{\varepsilon}^{z}_{H}$. Also, for the validation purpose of the material model adopted into the proposed formulation, the experimental results provided by Arruda et al. (1995) is plotted in Fig. 5(d). Meanwhile, Fig. 6 shows the relationship between the temperature and true compressive strain computed in response to each strain rate in conjunction with the experimental data provided by Arruda et al. (1995). In addition, the responses of Node A are extracted and plotted in the bottom right side of the figure (Fig. 6(d)). As can be seen from the results of the case with $\dot{\varepsilon}^{z}_{H} = -0.001\ [s^{-1}]$ in Fig. 5(a), all the stresses differ little from each other and exhibit almost the same as that of the case with 25.0 [deg] in Fig. 2. This must be due to the low deformation rate that causes little temperature increases as shown in Fig. 6(a). In fact, the maximum temperature elevation is about 3.0 [K], so that the isothermal process is approximately realized over the whole specimen.

On the other hand, as can be seen from Fig. 5(b) and (c), the results of the cases with higher compressive strain rates of $\dot{\varepsilon}^{z}_{H} = -0.01$ and $-0.1\ [s^{-1}]$ indicate that each of the stresses rapidly decreases after the local maximum point and the decrement is much larger than those of the case with the lowest deformation rate shown in Fig. 5(a). This is caused mainly by the stiffness reduction due to the elevated temperature in addition to the strain softening associated with the intermolecular resistance as mentioned in subsection 5.1.1. In fact, this kind of behavior has also been reported in the literature (Arruda et al., 1995), which states that the higher the compression rate, the larger the temperature elevation. This statement can be confirmed from our calculation results as shown in Fig. 6(d). At the same time, the orientation hardening responses also tend to be suppressed or disappeared in the cases with higher strain rates. However, the stress responses of Element IV seem to be exceptional. Also, in response to this, the temperature elevations of Node E adjacent to Element IV are smaller than those of the other nodes. The reason is that the self-generated heat in this element quickly transfers to the steel attachment because of the large heat conductivity of the steel. In other words, Element IV is the farthest from an adiabatic state among the target elements.

As can be seen from Fig. 5(d), the simulated mechanical responses are in some agreement with experimental ones, even though they may not be satisfactory. In particular, it can be confirmed from the numerical results that the magnitude relationship among the stresses with different compression speeds is reversed during the strain hardening, which is the same tendency as the experimental one. However, the slope of the increase in simulated true stress during the strain softening is steeper than experimental

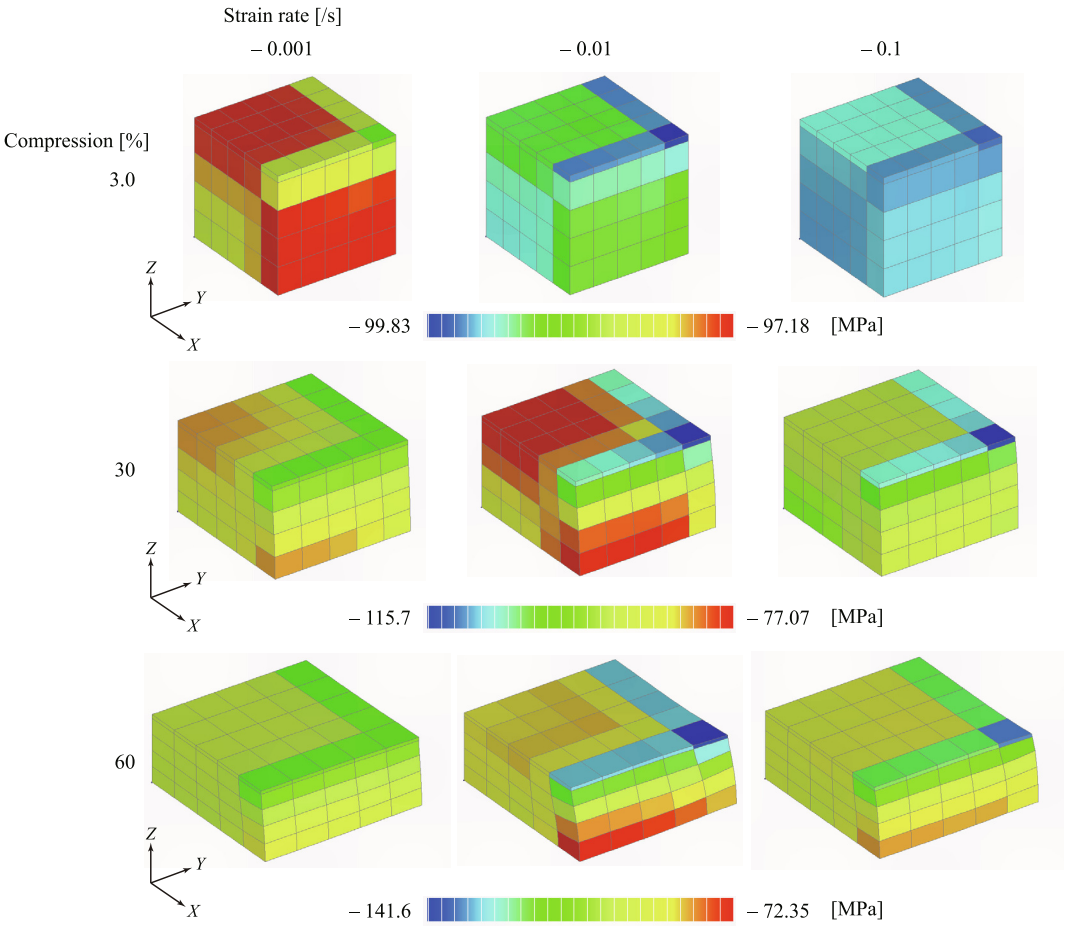

Fig. 7. Deformed configurations with distributions of normal stress in Z-direction for three levels of true strain rates.

one. It is probably due to the fact that the simulated temperatures attain local maximum earlier than experimental results as shown in Fig. 6. This tendency indeed reflects the discrepancy between temperature evolutions in the numerical analysis and the experiment. A possible modification is to introduce a free volume change into the evolution law of the yield strength (Anand and Gurtin, 2003) or/and a more sophisticated overstress model, but is left for future work.

Figs. 7 and 8 show the deformed configurations with the contours of normal stresses in the Z and Y directions, respectively, which are three snapshots at $\tilde{\varepsilon}^z_{\mathrm{H}} = -3.0, -30, -60[\%]$ during the compression process. Also, Fig. 9 illustrates the corresponding temperature distributions drawn in the deformed configurations. For each level of deformation, we investigate the interaction between mechanical and thermal responses below by making a detailed observation of the local stresses and temperatures as well as the overall deformations.

First, we focus our attention to the state of $\tilde{\varepsilon}^z_{\mathrm{H}} = -3.0$ [%], in which all the elements have not attained the local maximum stress yet. In this low level of deformation, the distributions of normal stress in the Z-direction are almost uniform in all the cases with different strain rates. In fact, the largest difference in stress is about 2.7 [MPa] and observable in Fig. 7. In response to this, the self-generated heat occurs due to the entropy change associated with thermal expansion and thermo-elasticity, although the temperature distributions are also almost uniform. Their slight non-uniformity arises from both the non-uniformities of the corresponding stresses and the heat transfer on the external boundaries and induces the onset of inhomogeneous thermal expansion in the transverse direction. In fact, the latter effect seems to be more perceptible from the upper row of Fig. 9.

Second, we direct our eyes on the stress distributions at the stage of 30 [%] compression shown in the middle rows of Figs. 7 and 8, which correspond to the states in which the softening almost ceases. Once the strain softening occurs, the viscoplastic flow suddenly dominates the deformation. As can be seen, the non-uniformity becomes prominent. This can be explained by the corresponding temperature distributions, which are illustrated in the middle row of Fig. 9. That is, the specimen exhibits the temperature elevation up to over 25 [K] and the order of elevation rates is in accord with that of applied strain rates. These elevations are mainly due to the large inelastic deformations, although some effect of entropy change remains. At the same time, the non-uniformity in temperature distribution is noticeable in each of the figures owing to the heat transfer on the external surfaces. In particular, in the case of $\dot{\varepsilon}^z_{\mathrm{H}} = -0.01\ [\mathrm{s}^{-1}]$, both the non-negligible heat transfer and relatively low conductivity of PMMA enlarges the temperature difference between the central part and external boundaries of the specimen. As a result, the temperature-dependent material properties take different values despite the original homogeneity and then make the stress distribution non-uniform. On the other hand, the self-generated heat seems large enough in the case of $\dot{\varepsilon}^z_{\mathrm{H}} = -0.1\,[\mathrm{s}^{-1}]$, so that its heat release rate cannot be overtaken by the speed of heat transfer. As a result, the non-uniformity in temperature distribution is not so prominent in comparison with that of the case of $\dot{\varepsilon}^z_{\mathrm{H}} = -0.01\ [\mathrm{s}^{-1}]$.

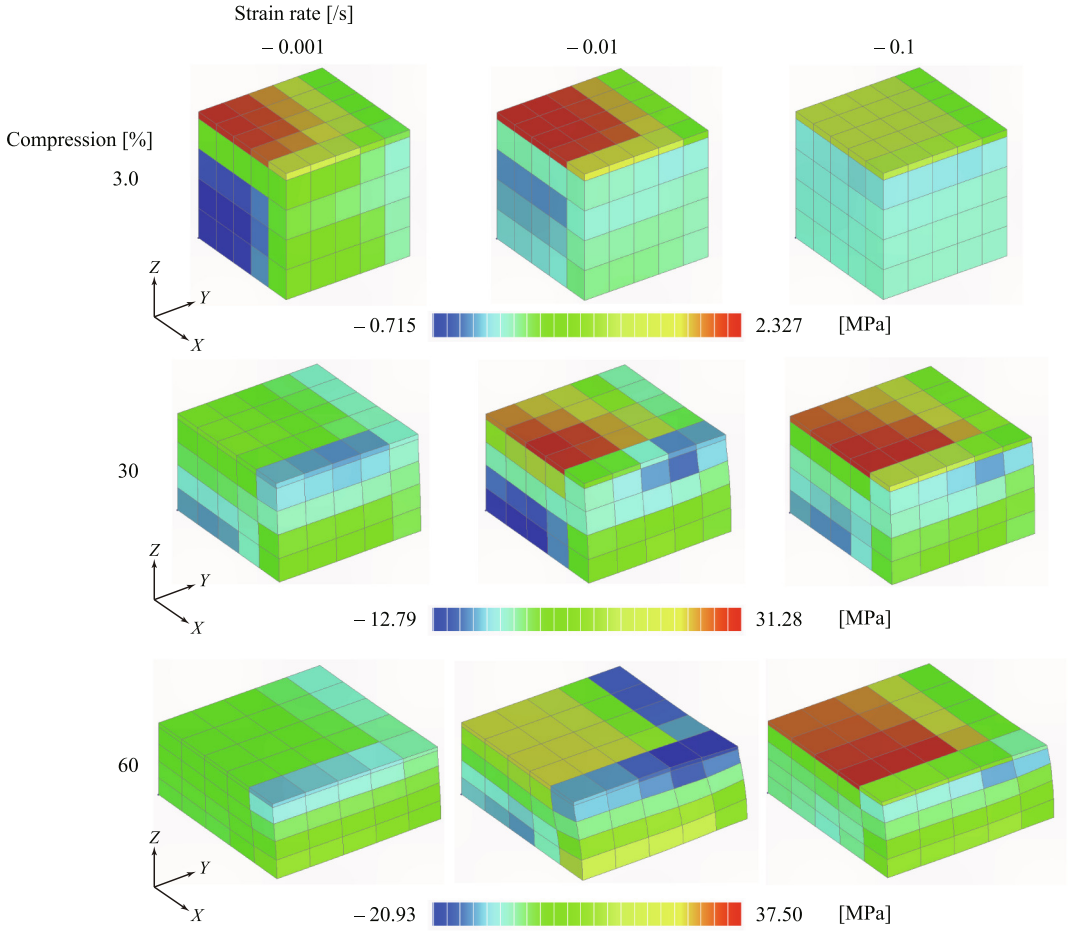

Fig. 8. Deformed configurations with distributions of normal stress in Y-direction for three levels of true strain rates.

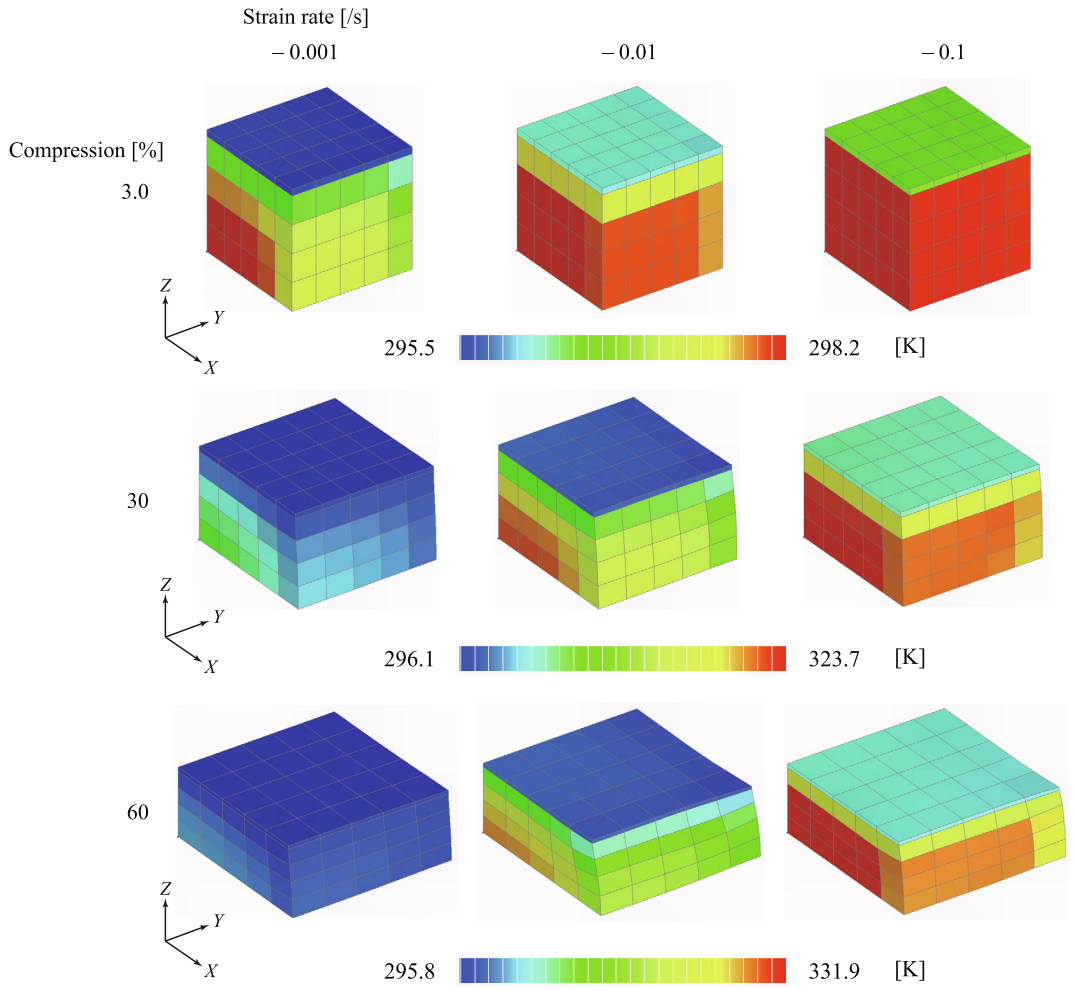

Fig. 9. Deformed configurations with distributions of temperature for three levels of true strain rates.

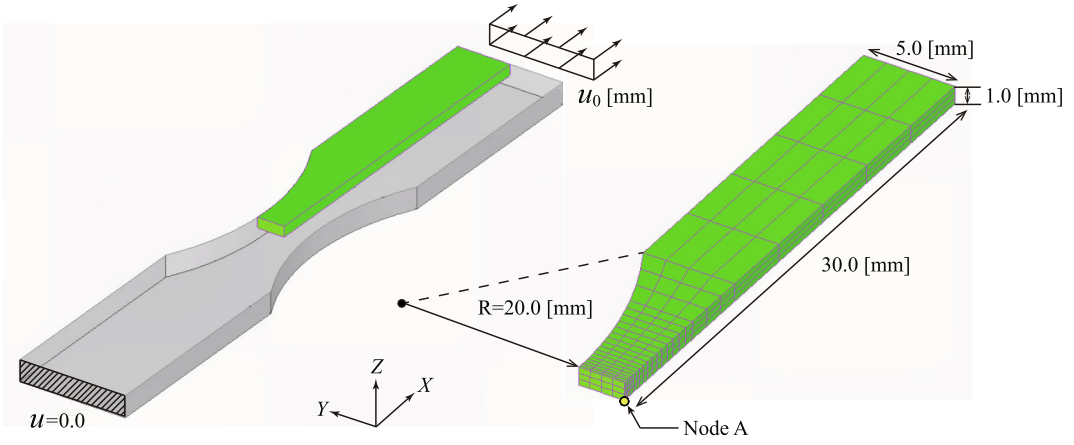

(a) R-20-type notched specimen (b) FE model of one-eighth the specimen

Fig. 10. R-20-type notched specimen and FE model.

The last investigation is conducted on the states of the specimen further compressed up to −60 [%] apparent strain, which are illustrated in the bottom row of Figs. 7 and 8, As can be seen from these figures, the non-uniform stress distributions make the barreled deformed shapes noticeable. This peculiar behavior reflects the highly-developed non-uniformity of the temperature distributions, which are shown in the bottom row of Fig. 9. More specifically, the no-way-out heat in the heart of the specimen causes relatively high temperatures around the mid plane that corresponds to the symmetry plane perpendicular to the Z-axis, whereas the temperature distributions around the top surface are close to room temperature due to the high heat conductivity of

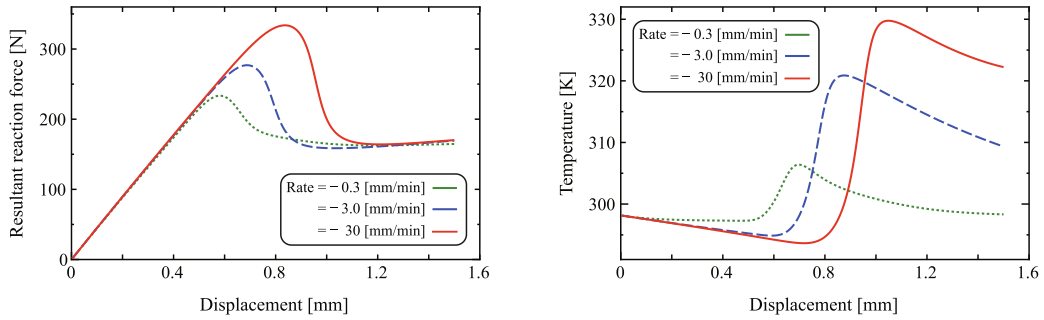

(a) Relationships between reaction forces and enforced displacements (b) Relationships between temperatures and enforced displacements

Fig. 11. Resultant reaction forces and temperatures versus enforced displacements.

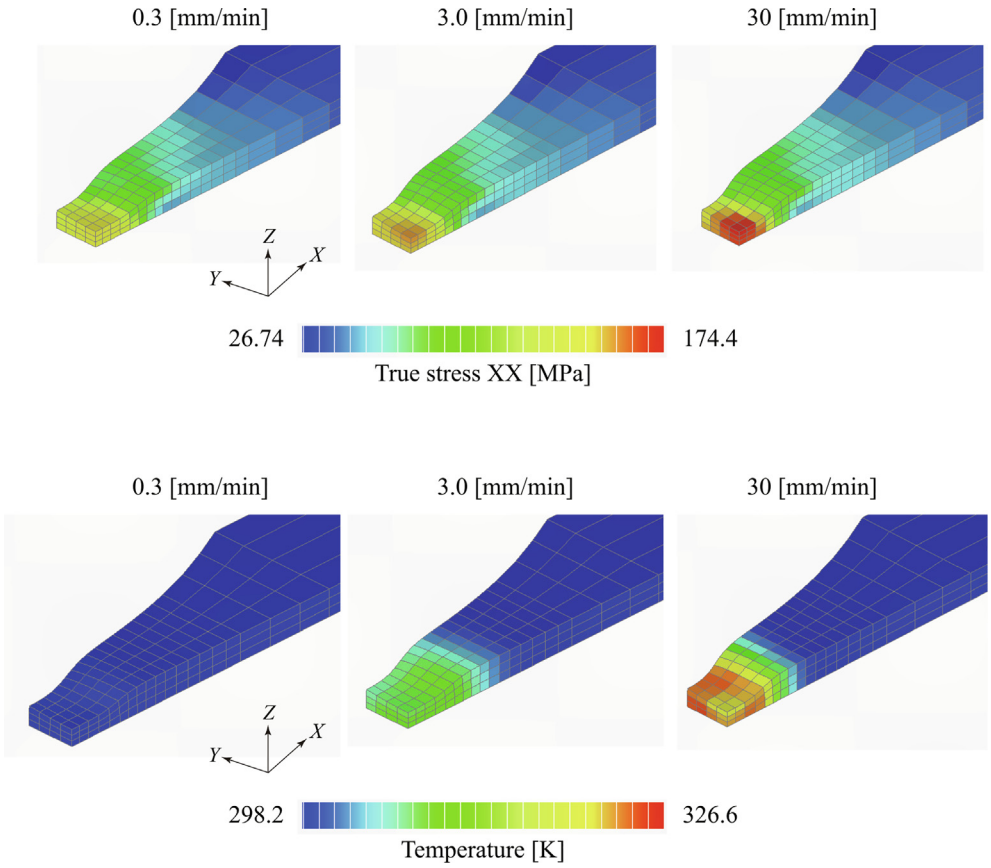

Fig. 12. Deformed configurations with stress and temperature distributions at the end of elongation.

the steel. It should be noted here that the higher the temperature, the lower the stiffness, in general and for this particular resin material. In response, relatively high stresses distribute around the region of low temperature and correspond to the responses of Element IV in Fig. 5. In particular, the difference between the maximum and minimum values of the normal stress in the Z-direction attains about 70 [MPa]. On the contrary, in the case of the smallest compression speed, almost uniform stress distributions remain unchanged even in the 60[%] compression state, because sufficient time is given to the specimen to keep the uniform temperature distributions throughout the deformation process.

In summary, the non-uniform stress distributions are triggered by the reductions of stiffness and yield strength due to the non-uniform temperature distributions at the early stage of deformation, which are mainly caused by the entropy change. At the intermediate range of deformation, the non-uniform stress distributions induced by the non-uniformity in temperature become prominent especially in the case of intermediate strain rate. Here, the main source of heat conduction is the self-generated heat due to large inelastic deformations, and the non-uniform temperature distributions are caused by the heat transfer on the external boundaries. These non-uniform stresses facilitate the barrel-shaped deformations of the specimen at the last stage of the simulation. The bulge around the middle part of the specimen reflects the low stiffness that is caused by the no-way-out heat near the interior mid plane. Nevertheless, the degrees of non-uniformities in stress and temperature are determined by

the balance between the rates of heat generation and dissipation to into the media outside the specimen, both of which obviously depend on the imposed deformation rates.

The fully coupled phenomena in the thermo-mechanical problem for glassy amorphous polymers have successfully been predicted by the standard FEM enhanced by the novel formulation based on the incremental variational principle. The conventional strong coupling schemes should also be capable of simulating such phenomena, but are generally time-consuming when a staggered algorithm is adopted, for example, and require much more effort for implementation and computation than necessary. In contrast, the proposed formulation is easy to implement thanks to both the proposed incremental variational formulation for non-associative viscoplasticity and the variationally consistent constitutive equations for glassy amorphous polymers. It is worth mentioning that this feature is particularly beneficial to other non-associative viscoplastic models. Also, the monolithic method realized for thermo-mechanically coupled analyses in this study makes computations relatively stable in comparison with the conventional approaches. It seems, therefore, reasonable to conclude that the achievements in this study offer a superior scheme against the conventional ones.

It should be noted, however, that the material instability associated with the strain softening results from the adopted constitutive law and makes the convergence characteristic poor in solving the global equilibrium equations. When the necking behavior of a tensile specimen is simulated, such an instability commonly becomes prominent and generates a harmful effect on the global convergence; see Appendix A for the demonstration. Nevertheless, since any issue caused by the material instability is irrelevant to the proposed formulation, we leave such a treatment for our future work at the moment.

6. Conclusion

This study present a variationally consistent formulation of the thermo-mechanically coupled problems with non-associative viscoplasticity for glassy amorphous polymers. For that purpose, we have proposed an alternative form of the dual dissipation potential to realize the variationally consistent constitutive model in non-associative viscoplasticity. Specifically, the principle of maximum plastic dissipation for viscoplasticity is recasted into the same form of rate-independent plasticity by the introduction of the extended yield function and by the application of the parameterization of flow rules. During the course of the formulation, the decomposition of the equivalent plastic strain is a key to derive the variational consistent evolution law of the shear yield strength with reference to the analogous approach taken for formulating the Armstrong-Frederick model. As the result, the proposed formulation does not require the time derivative of the shear yield strength to derive its evolution equation, while the time derivative is indispensable in the conventional ones. Owing to this characteristic feature, the resulting evolution equation accommodates the time variations of temperature in terms of its material properties, implying that it is amenable to various thermal processes other than isothermal ones.

The numerical example presented in this study is rather simple at first glance, but fairly complex in reality. Indeed, it is sufficiently demonstrative in simulating typical thermo-mechanically coupled phenomena of a largely deforming structure made of a glassy amorphous polymer that is subjected to different deformation rates. Even though no external heat is supplied, the heat is generated at each material point in the target structure due to both the entropy change associated with thermal expansion as well as thermo-elasticity and large viscoplastic strains. However, because of the heat conduction along with various boundary conditions, the evolution of temperature varies considerably by location in the structure. As a result, the obtained temperature distributions are non-uniform and vary with the imposed deformation rates. Each of these non-uniformities causes different material responses by location and makes the overall deformation of the structure non-uniform despite the loading is originally intended to realize the uniformity in deformation. It is worthwhile to note that the mathematical model derived by the proposed formulation enables us to not only successfully characterize the complex thermo-mechanical behavior, but also provides a strictly strong coupling scheme to solve the thermo-mechanically coupled problem in an efficient way.

Declaration of Competing Interest

The authors declare that they have no known competing financial interests or personal relationships that could have appeared to influence the work reported in this paper.

Acknowledgement

This work was partially supported by The Japan Society for the Promotion of Science (JSPS) under Grant-in-Aid for Early-Career Scientists (20K14603).

Appendix A. Tensile tests of R-20-type notched specimen

To further demonstrate the performance of the present model, FE-analyses for the tensile tests of R-20-type notched specimen are conducted here by reference to Matsubara et al. (2020). Fig. 10(a) shows the R-20-type notched specimen subjected to tensile loading and Fig. 10(b) shows the prepared FE model of one-eighth of the specimen, on which the symmetric condition is imposed. The specimen is elongated with an enforced displacement of $u_0 = 1.5$ [mm] with 3 different deformation rates.

Fig. 11 shows the resultant reaction forces and the temperatures at Node A depicted in Fig. 10 versus the enforced displacements. As can be seen from these figures, all the resultant reaction forces drastically decrease within a range of $u_0 = 0.5 \sim 1.0$ [mm] and the maximum temperature attains about 330 [K] in the case with the highest deformation rate. Also, Fig. 12 shows the deformed configurations with stress and temperature distributions at the end of elongation. As can be seen from each of the figures, once the strain concentrates near the center of the specimen, the deformation propagates toward the edge of specimen. Yet, the strain hardening develops, so that the resultant reaction force becomes almost constant and at the same time the temperature change shift to decrease. This series of responses typifies the material instability due to the strain softening, which is caused by the adopted constitutive law. In this way, the tensile behavior of the glassy amorphous polymer can also be successfully simulated with the solution method realized by the proposed formulation.

References

Ames, N.M., Srivastava, V., Chester, S.A., Anand, L., 2009. A thermo-mechanically coupled theory for large deformations of amorphous polymers. part ii: Applications. International Journal of Plasticity 25, 1495–1539. https://doi.org/10.1016/j.ijplas.2008.11.005.

Anand, L., Gurtin, M.E., 2003. A theory of amorphous solids undergoing large deformations with application to polymeric glasses. International Journal of Solids and Structures 40, 1465–1487. https://doi.org/10.1016/S0020-7683(02)00651-0.

Anand, L., Ames, N.M., Srivastava, V., Chester, S.A., 2009. A thermo-mechanically coupled theory for large deformations of amorphous polymers. part i:

Formulation. International Journal of Plasticity 25, 1474–1494. https://doi.org/10.1016/j.ijplas.2008.11.004.
Argon, A.S., 1973. A theory for the low-temperature plastic deformation of glassy polymers. Philosophical Magazine 28, 839–865. https://doi.org/10.1080/14786437308220987.
Arruda, E.M., Boyce, M.C., 1993a. Evolution of plastic anisotropy in amorphous polymers during finite straining. International Journal of Plasticity 9, 697–720. https://doi.org/10.1016/0749-6419(93)90034-N.
Arruda, E.M., Boyce, M.C., 1993b. A three-dimensional constitutive model for the large stretch behavior of rubber elastic materials. Journal of the Mechanics and Physics of Solids 41 (2), 389–412. https://doi.org/10.1016/0022-5096(93)90013-6.
Arruda, E.M., Boyce, M.C., Jayachandran, R., 1995. Effects of strain rate, temperature and thermomechanical coupling on the finite strain deformation of glassy polymers. Mechanics of Materials 19 (2–3), 193–212. https://doi.org/10.1016/0167-6636(94)00034-E.
Balzani, D., Ortiz, M., 2012. Relaxed incremental variational formulation for damage at large strains with application to fiber-reinforced materials and materials with truss-like microstructures. International Journal for Numerical Methods in Engineering 92 (6), 551–570. https://doi.org/10.1002/nme.4351.
Bleier, N., Mosler, J., 2012. Efficient variational constitutive updates by means of a novel parameterization of the flow rule. International Journal for Numerical Methods in Engineering 89, 1120–1143. https://doi.org/10.1002/nme.3280.
Bleier, N., Mosler, J., 2013. A hybrid variationally consistent homogenization approach based on ritz's method. International Journal for Numerical Methods in Engineering 94, 625–647. https://doi.org/10.1002/nme.4465.
Bouvard, J.L., Francis, D.K., Tschopp, M.A., Marin, E.B., Bammann, D.J., Horstemeyer, M.F., 2013. An internal state variable material model for predicting the time, thermomechanical, and stress state dependence of amorphous glassy polymers under large deformation. International Journal of Plasticity 42, 168–193. https://doi.org/10.1016/j.ijplas.2012.10.005.
Boyce, M.C., 1996. Direct comparison of the Gent and the Arruda-Boyce constitutive models of rubber elasticity. Rubber Chemistry and Technology 69 (5), 781–785. https://doi.org/10.5254/1.3538401.
Boyce, M.C., Parks, D.M., Argon, A.S., 1988a. Large inelastic deformation of glassy polymers. parti: Rate dependent constitutive model. Mechanics of Materials 7, 15–33. https://doi.org/10.1016/0167-6636(88)90003-8.
Boyce, M.C., Parks, D.M., Argon, A.S., 1988b. Large inelastic deformation of glassy polymers. partii: Numerical simulation of hydrostatic extrusion. Mechanics of Materials 7, 35–47. https://doi.org/10.1016/0167-6636(88)90004-X.
Canadija, M., Mosler, J., 2011. On the thermomechanical coupling in finite strain plasticity theory with non-linear kinematic hardening by means of incremental energy minimization. International Journal of Solids and Structures 48 (7), 1120–1129. https://doi.org/10.1016/j.ijsolstr.2010.12.018.
Canadija, M., Mosler, J., 2016. A variational formulation for thermomechanically coupled low cycle fatigue at finite strains. International Journal of Solids and Structures 100–101, 388–398. https://doi.org/10.1016/j.ijsolstr.2016.09.009.
Carstensen, C., Hackl, K., Mielke, A., 2002. Non-convex potentials and microstructures in finite-strain plasticity. Proceedings of the Royal Society, Series A 458, 299–317. https://doi.org/10.1098/rspa.2001.0864.
Chaboche, J.L., 1986. Time-independent constitutive theories for cyclic plasticity. International Journal of Plasticity 2, 149–188. https://doi.org/10.1016/0749-6419(86)90010-0.
Chaboche, J.L., 1989. Constitutive equations for cyclic plasticity and cyclic viscoplasticity. International Journal of Plasticity 5, 247–302. https://doi.org/10.1016/0749-6419(89)90015-6.
Coleman, B.D., Gurtin, M.E., 1967. Thermodynamics with internal state variables. The Journal of Chemical Physics 47, 597–613. https://doi.org/10.1063/1.1711937.
Coleman, B.D., Noll, W., 1963. The thermodynamics of elastic materials with heat conduction and viscosity. Archive for Rational Mechanics and Analysis 13, 167–178. https://doi.org/10.1007/BF01262690.
Comi, C., Perego, U., 1995. A unified approach for variationally consistent finite elements in elastoplasticity. Computer Methods in Applied Mechanics and Engineering 121 (1–4), 323–344. https://doi.org/10.1016/0045-7825(94)00703-P.
Comi, C., Corigliano, A., Maier, G., 1991. Extremum properties of finite-step solutions in elastoplasticity with nonlinear hardening. International Journal for Solids and Structures 27 (8), 965–981. https://doi.org/10.1016/0020-7683(91)90094-V.
Dettmer, W., Reese, S., 2003. On the theoretical and numerical modelling of armstrong-frederick kinematic hardening in the finite strain regime. Computer Methods in Applied Mechanics and Engineering 193, 87–116. https://doi.org/10.1016/j.cma.2003.09.005.
Fancello, E., Ponthot, J.P., Stainier, L., 2006. A variational formulation of constitutive models and updates in non-linear finite viscoelasticity. International Journal for Numerical Methods in Engineering 65 (11), 1831–1864. https://doi.org/10.1002/nme.1525.
Fancello, E.A., Ponthot, J.P., Stainier, L., 2008. A variational framework for nonlinear viscoelastic models in finite deformation regime. Journal of Computational and Applied Mathematics 215, 400–408. https://doi.org/10.1016/j.cam.2006.04.064.
Farias, J.M.C., Stainier, L., Fancello, E.A., 2019. A variational framework for the modeling of glassy polymers under finite strains. Continuum Mechanics and Thermodynamics 32, 1037–1055. https://doi.org/10.1007/s00161-019-00809-8.
Flory, P.J., 1961. Thermodynamics relations for high elastic materials. Transactions of the Faraday Society 57, 829–838. https://doi.org/10.1039/TF9615700829.
Fotheringham, D.G., Cherry, B.W., 1978. The role of recovery forces in the deformation of linear polyethylene. Journal of Materials Science 13, 951–964. https://doi.org/10.1007/BF00544690.
Gent, A.N., 1996. A new constitutive relation for rubber. Rubber Chemistry and Technology 69, 59–61. https://doi.org/10.5254/1.3538357.
Halphen, B., Nguyen, Q.S., 1975. Sur les materiaux standards generalises. Journal de Mecanique 14, 39–63.
Haward, R.N., Thackray, G., 1968. The use of a mathematical model to describe isothermal stress-strain curves in glassy thermoplastics. Proceedings of the Royal Society of London A: Mathematical, Physical and Engineering Sciences 302, 453–472. https://doi.org/10.1098/rspa.1968.0029.
Henann, D.L., Anand, L., 2008. A large deformation theory for rate-dependent elastic-plastic materials with combined isotropic and kinematic hardening. International Journal of Plasticity 25, 1833–1878. https://doi.org/10.1016/j.ijplas.2008.11.008.
Kröner, E., 1960. Allgemeine kontinuumstheorie der versetzungen und eigenspannungen. Archive for Rational Mechanics and Analysis 4, 273–334. https://doi.org/10.1007/BF00281393.
Lee, E.H., 1969. Elastic plastic deformation at finite strain. ASME Journal of Applied Mechanics 36, 16. https://doi.org/10.1115/1.3564580.
Lion, A., 1999. Constitutive modelling in finite thermoviscoplasticity: a physical approach based on nonlinear rheological models. International Journal of Plasticity 16, 469–494. https://doi.org/10.1016/S0749-6419(99)00038-8.
Matsubara, S., Terada, K., Maeda, R., Kobayashi, T., Murata, M., Sumiyama, T., Furuichi, K., Nonomura, C., 2020. Viscoelastic-viscoplastic combined constitutive model for glassy amorphous polymers under loading/unloading/no-load states. Engineering Computations 37 (5), 1703–1735. https://doi.org/10.1108/EC-05-2019-0197.
Mosler, J., 2010. Variationally consistent modeling of finite strain plasticity theory with non-linear kinematic hardening. Computer Methods in Applied Mechanics and Engineering 199, 2753–2764. https://doi.org/10.1016/j.cma.2010.03.025.
Mosler, J., Bruhns, O.T., 2008. Towards variational constitutive updates for non-associative plasticity models at finite strain: models based on a volumetric-deviatoric split. International Journal of Solids and Structures 46 (7), 1676–1684. https://doi.org/10.1016/j.ijsolstr.2008.12.008.
Mosler, J., Bruhns, O.T., 2010. On the implementation of rate-independent standard dissipative solids at finite strain – variational constitutive updates. Computer Methods in Applied Mechanics and Engineering 199, 417–429. https://doi.org/10.1016/j.cma.2009.07.006.
Ortiz, M., Stainier, L., 1999. The variational formulation of viscoplastic constitutive updates. Computer Methods in Applied Mechanics and Engineering 171 (3–4), 419–444. https://doi.org/10.1016/S0045-7825(98)00219-9.
Richeton, J., Ahzi, S., Daridon, L., Remond, Y., 2005. A formulation of the cooperative model for the yield stress of amorphous polymers for a wide range of strain rates and temperatures. Polymer 46, 6035–6043. https://doi.org/10.1016/j.polymer.2005.05.079.
Richeton, J., Ahzi, S., Vecchio, K.S., Jiang, F.C., Adharapurapu, R.R., 2006. Influence of temperature and strain rate on the mechanical behavior of three amorphous polymers: Characterization and modeling of the compressive yield stress. International Journal of Solids and Structures 43, 2318–2335. https://doi.org/10.1016/j.ijsolstr.2005.06.040.
Richeton, J., Ahzi, S., Vecchio, K.S., Jiang, F.C., Makradi, A., 2007. Modeling and validation of the large deformation inelastic response of amorphous polymers over a wide range of temperatures and strain rates. International Journal of Solids and Structures 44, 7938–7954. https://doi.org/10.1016/j.ijsolstr.2007.05.018.
Yang, Q., Stainier, L., Ortiz, M., 2005. A variational formulation of the coupled thermo-mechanical boundary-value problem for general dissipative solids. Journal of the Mechanics and Physics of Solids 54 (2), 401–424. https://doi.org/10.1016/j.jmps.2005.08.010.
Simo, J.C., Hughes, T.J.R., 2006. Computational inelasticity, Vol. 7, Springer Science & Business Media. doi:10.1007/b98904..
Srivastava, V., Chester, S.A., Ames, N.M., Anand, L., 2010. A thermo-mechanically-coupled large-deformation theory for amorphous polymers in a temperature range which spans their glass transition. International Journal of Plasticity 26, 1138–1182. https://doi.org/10.1016/j.ijplas.2010.01.004.
Stainier, L., Ortiz, M., 2010. Study and validation of a variational theory of thermo-mechanical coupling in finite visco-plasticity, International Journal of Solids and Structures 47 (5), 705–515. doi:10.1016/j.ijsolstr.2009.11.012..
Tanaka, M., Balzani, D., Schroder, J., 2016. Implementation of incremental variational formulations based on the numerical calculation of derivatives using hyper dual numbers. Computer Methods in Applied Mechanics and Engineering 301 (1), 216–241. https://doi.org/10.1016/j.cma.2015.12.010.
Vladimirov, I.N., Pietryga, M.P., Reese, S., 2007. On the modelling of non-linear kinematic hardening at finite strains with application to springback – comparison of time integration algorithms. International Journal for Numerical Methods in Engineering 75, 1–28. https://doi.org/10.1002/nme.2234.
Vladimirov, I.N., Pietryga, M.P., Reese, S., 2010. Anisotropic finite elastoplasticity with nonlinear kinematic and isotropic hardening and application to sheet metal forming. International Journal of Plasticity 26, 659–687. https://doi.org/10.1016/j.ijplas.2009.09.008.
Ward, I.M., Sweeney, J., 2013. Mechanical properties of solid polymers: Third edition, John Wiley & Sons Ltd, 2013. doi:10.1002/9781119967125..